Nanostructures

DOI: 10.1002/anie.200603148

Synthesis of Monodisperse Spherical Nanocrystals

*Jongnam Park, Jin Joo, Soon Gu Kwon, Youngjin Jang, and Taeghwan Hyeon**

Keywords:
gold · magnetic nanocrystals · monodisperse nanocrystals · noble metals · quantum dots · semiconductors

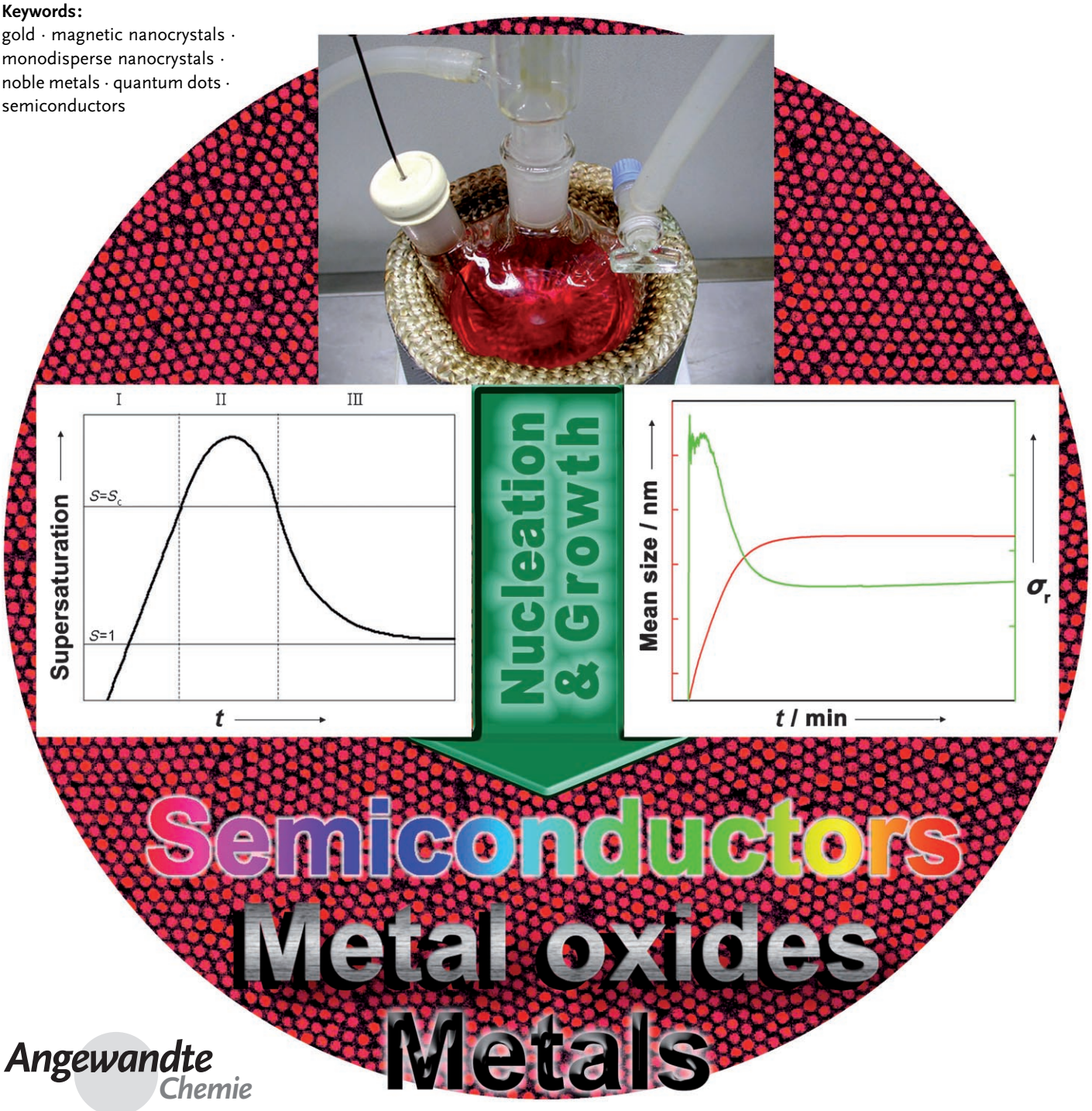

Much progress has been made over the past ten years on the synthesis of monodisperse spherical nanocrystals. Mechanistic studies have shown that monodisperse nanocrystals are produced when the burst of nucleation that enables separation of the nucleation and growth processes is combined with the subsequent diffusion-controlled growth process through which the crystal size is determined. Several chemical methods have been used to synthesize uniform nanocrystals of metals, metal oxides, and metal chalcogenides. Monodisperse nanocrystals of CdSe, Co, and other materials have been generated in surfactant solution by nucleation induced at high temperature, and subsequent aging and size selection. Monodisperse nanocrystals of many metals and metal oxides, including magnetic ferrites, have been synthesized directly by thermal decomposition of metal–surfactant complexes prepared from the metal precursors and surfactants. Nonhydrolytic sol–gel reactions have been used to synthesize various transition-metal-oxide nanocrystals. Monodisperse gold nanocrystals have been obtained from polydisperse samples by digestive-ripening processes. Uniform-sized nanocrystals of gold, silver, platinum, and palladium have been synthesized by polyol processes in which metal salts are reduced by alcohols in the presence of appropriate surfactants.

From the Contents

1. Introduction

Over the last 30 years, the synthesis of nanocrystals—crystalline particles ranging in size from 1 to 100 nm—has been intensively pursued, not only for their fundamental scientific interest, but also for their many technological applications.[1] Nanocrystals exhibit very interesting size-dependent electrical, optical, magnetic, and chemical properties that cannot be achieved by their bulk counterparts. For many future applications, the synthesis of uniform-sized nanocrystals (monodisperse with a size distribution $\sigma_r \leq 5\%$) is of key importance, because the electrical, optical, and magnetic properties of these nanocrystals are strongly dependent on their dimensions. The most popular demonstration of the size-dependent characteristics of nanocrystals is the continuous fluorescent emission from semiconductor nanocrystals (also known as quantum dots (QDs)) which covers the entire visible spectrum as a function of their size.[1c] For applications in optical devices, size uniformity is critical for achieving a sharp colored emission. Monodisperse magnetic nanocrystals are essential for the next-generation multi-terabit (Tbit/in^2) magnetic storage media.[1e,2]

There are two different approaches to synthesize nanocrystals: the "top-down" approach, which utilizes physical methods, and the "bottom-up" approach, which employs solution-phase colloidal chemistry.[1] The advantage of the physical methods is the production of a large quantity of nanocrystals, whereas the synthesis of uniform-sized nanocrystals and their size control is very difficult to achieve by using the top-down approach. In contrast, colloidal chemical synthetic methods can be used to synthesize uniform nanocrystals with controlled particle size, although generally only subgram quantities are produced. Furthermore, various-shaped nanocrystals, including nanorods and nanowires, can be synthesized by varying the reaction conditions such as the use of a mixture of surfactants. This Review focuses primarily on the advances made over the last ten years on the synthesis of monodisperse spherical nanocrystals with diameters ranging from 2 to 20 nm by colloidal chemical approaches. The synthesis of nanocrystals, including nanorods and nanowires,[3a,b] has been well documented in several review articles.[3] More recently, Cheon and co-workers reviewed the shape-controlled synthesis of nanocrystals of metal oxides and semiconductors through nonhydrolytic colloidal routes.[3d]

We first summarize the formation mechanism of monodisperse spherical nanoparticles and then the various synthetic procedures for nanoparticles. In the following sections, we review the synthesis of monodisperse nanocrystals of various kinds of materials according to their compositions.

2. Formation Mechanism of Monodisperse Nanocrystals

Understanding the mechanism of formation of monodisperse nanocrystals is very important because it will help us to

[*] Dr. J. Park, Dr. J. Joo, S. G. Kwon, Y. Jang, Prof. Dr. T. Hyeon
National Creative Research Initiative Center
for Oxide Nanocrystalline Materials, and
School of Chemical and Biological Engineering
Seoul National University
Seoul 151-744 (Korea)
Fax: (+82) 2-886-8457
E-mail: thyeon@snu.ac.kr

develop improved synthetic methods that can be generally applicable to various kinds of materials. Although several colloidal chemical methods have been developed to synthesize monodisperse nanocrystals of various materials, gaining a comprehensive understanding of how monodisperse nanoparticles form is still very challenging. In this section, we summarize the crystallization (both nucleation and growth) mechanism for monodisperse nanocrystals. Some formation mechanisms for the monodisperse micrometer-sized particles work quite well for monodisperse nanocrystals. However, it is much more difficult to elucidate the mechanism for nanometer-sized particles because of their high surface-to-volume ratios. Although the nucleation and growth processes are strongly correlated, we discuss these two processes separately for the sake of simplicity. We performed computer simulations to correlate and explain the previous experimental results for the formation of monodisperse CdSe nanocrystals.

2.1. Nucleation

2.1.1. Burst of Nucleation Concept

Research on the preparation of uniform colloidal particles dates back to the 1940s. LaMer and his colleagues pioneered the research by preparing various oil aerosols and sulfur hydrosols, and they proposed the concept of "burst nucleation."[4,5] In this process, many nuclei are generated at the same time, and then these nuclei start to grow without additional nucleation. Because all of the particles nucleate almost simultaneously, their growth histories are nearly the same. This is the essence of the "burst-nucleation" process which makes it possible to control the size distribution of the ensemble of particles as a whole during growth. Otherwise, if nucleation process occurred throughout the particle-formation process, the growth histories of the particles would differ largely from one another, and consequently the control of the size distribution would be very difficult (control of the size distribution during the growth process is discussed in Section 2.2).

"Burst nucleation" has been adopted as an important concept in the synthesis of monodisperse nanocrystals. It is well known that to prepare highly uniform nanocrystals it is necessary to induce a single nucleation event and to prevent additional nucleation during the subsequent growth process. As a synthetic strategy, this method is often referred to as "the separation of nucleation and growth."[5–7] LaMer and his colleagues utilized the homogeneous nucleation process to separate nucleation and growth. In the homogeneous nucleation process, nuclei appear in a homogeneous solution without any seed for heterogeneous nucleation (e.g., dust

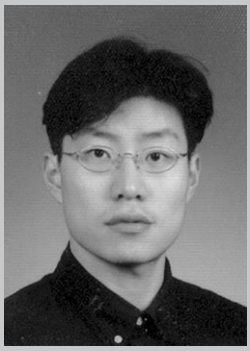

Jongnam Park received his BS (1999), MS (2001), and PhD (2005) from the School of Chemical and Biological Engineering of the Seoul National University, Korea. During his PhD course under the direction of Prof. Taeghwan Hyeon, he conducted research on the synthesis and characterization of monodisperse magnetic nanocrystals. Since 2005, he has been a postdoctoral researcher at the National Creative Research Center for Oxide Nanocrystalline Materials, where he studies the mechanism of formation of uniform magnetic nanocrystals.

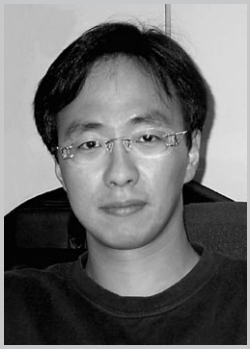

Jin Joo received his BS (1999), MS (2001), and PhD (2005) from the School of Chemical and Biological Engineering of the Seoul National University, Korea. During his graduate research under the direction of Prof. Taeghwan Hyeon, he worked on the synthesis of uniform-sized nanocrystals of metal oxides and metal sulfide nanocrystals. Since 2005, he has been working as a postdoctoral researcher at the National Creative Research Center for Oxide Nanocrystalline Materials on the synthesis of cadmium chalcogenide nanocrystals.

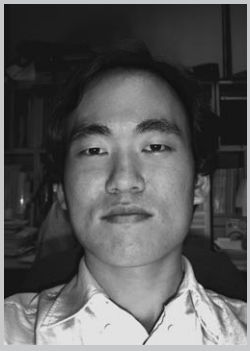

Soon Gu Kwon received his BS (2004) from the School of Chemical and Biological Engineering of the Seoul National University. He is now in a PhD course under the supervision of Prof. Taeghwan Hyeon. His research interests are focused on the syntheses of nanomaterials and the formation mechanism of monodisperse nanocrystals.

Youngjin Jang received his BS (2003) in chemical and biological engineering and MS (2005) from the Interdisciplinary Program in Nano-Science and Technology of the Seoul National University, Korea. Since then he has worked on his doctoral thesis under the direction of Prof. Taeghwan Hyeon focusing on the synthesis and characterization of monodisperse noble-metal nanocrystals.

Taeghwan Hyeon received his BS (1987) and MS (1989) in chemistry from the Seoul National University, Korea, and his PhD in chemistry from the University of Illinois at Urbana-Champaign (1996). He joined the faculty of the School of Chemical and Biological Engineering of Seoul National University in 1997, and is currently director of the National Creative Research Initiative Center for Oxide Nanocrystalline Materials. His research focuses on the synthesis and applications of uniform-sized nanocrystals and nanoporous carbon materials. He has received several awards, including the DuPont Science and Technology Award, and currently serves on the editorial boards of Advanced Materials, Small, and Chemical Communications.

particles or bubbles). In this homogeneous nucleation process, there exists a high energy barrier to nucleation, because the system spontaneously changes from the homogeneous phase to the heterogeneous phase. The LaMer plot, shown in Figure 1, is very useful for visualizing how the energy barrier

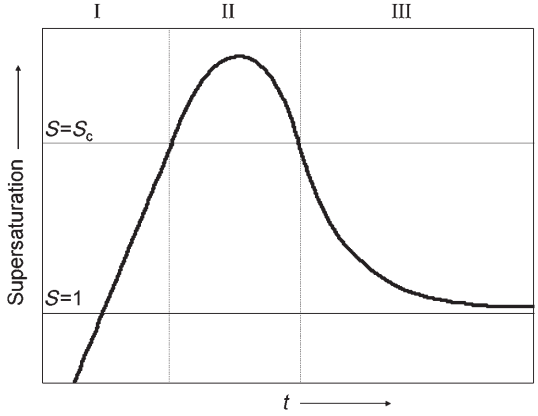

Figure 1. LaMer plot: Change of degree of supersaturation as a function of time.

works to induce the "burst nucleation."[5,7] The concentration of "monomer", which is the minimum subunit of bulk crystal, constantly increases with time. Note that precipitation does not occur in stage I even under supersaturated conditions ($S>1$), because the energy barrier for spontaneous homogeneous nucleation is extremely high. In stage II, during which nucleation occurs, the degree of supersaturation is high enough to overcome the energy barrier for nucleation, thus resulting in the formation and accumulation of stable nuclei. Since the rate of monomer consumption resulting from the nucleation and growth processes exceeds the rate of monomer supply, the monomer concentration decreases until it reaches the level at which the net nucleation rate (the number of nuclei formed per unit time) is zero. Below this level, the system enters the growth stage (stage III), in which nucleation is effectively stopped and the particles keep growing as long as the solution is supersaturated.

The energy barrier to the homogeneous nucleation is interpreted thermodynamically as follows: The Gibbs free energy of formation of spherical crystals with radius r from the solution with supersaturation S is given in Equation (1), in which γ is the surface free energy per unit area and ΔG_v is the free energy change between the monomers in the solution and unit volume of bulk crystal ($r\rightarrow\infty$).[8]

$$\Delta G = 4\pi r^2\gamma + \frac{4}{3}\pi r^3 \Delta G_v \tag{1}$$

γ is always positive and, because $\Delta G_v = (-RT\ln S)/V_m$ (V_m is the molar volume of bulk crystal), ΔG_v is negative as long as the solution is supersaturated. Consequently, a plot of ΔG versus r has a maximum. The value of r at which ΔG is maximum is called the critical radius r_c; this is the minimum radius of a nucleus that can grow spontaneously in the supersaturated solution. Setting $d\Delta G/dr = 0$ allows determination of r_c [Eq. (2)].

$$r_c = \frac{-2\gamma}{\Delta G_v} = \frac{2\gamma V_m}{RT\ln S} \tag{2}$$

Equation (2) imposes the first necessary condition for supersaturation with homogeneous nucleation. Because r_c is the minimum radius that will persist and not dissolve away in solution, S should be sufficiently high for r_c to be smaller than the size of the crystal embryos that form the nuclei for the homogeneous nucleation process.[9] Although little is known about the identity of the crystal embryos, their sizes might be less than 1 nm, which is comparable to the size of inorganic molecular clusters. Substituting Equation (2) into Equation (1) gives the critical free energy ΔG_c [Eq. (3)], which is the free energy necessary to form a stable nucleus.

$$\Delta G_c = \frac{16\pi\gamma^3}{3(\Delta G_v)^2} = \frac{16\pi\gamma^3 V_m{}^2}{3(RT\ln S)^2} \tag{3}$$

If the rate of increase of the number of particles N is defined as the rate of nucleation, it can be written in the Arrhenius form in terms of ΔG_c [Eq. (4)].[8]

$$\frac{dN}{dt} = A\exp\left[-\frac{\Delta G_c}{kT}\right] = A\exp\left[\frac{16\pi\gamma^3 V_m{}^2}{3k^3T^3N_A^2(\ln S)^2}\right] \tag{4}$$

At this point, it should be noted that, in contrast to the simple LaMer plot, it is hard to define exactly the critical supersaturation level at which nucleation begins, because nucleation and redissolution can happen at any concentration, as a result of the energy fluctuation in the solution.[4a] In fact, the nucleus can still form even in unsaturated solution, and the particles formed could redissolve unless they are stable enough to resist the free energy fluctuation of their surroundings. However, from the practical point of view, it is reasonable to establish the critical supersaturation level (S_c) at which stable nuclei form in an appreciable number per unit time and start to accumulate. To see how this condition affects S, we rewrite Equation (4) so as to express S in terms of $\dot{N}$ ($=dN/dt$) [Eq. (5)].

$$\ln S = \left[\frac{16\pi\gamma^3 V_m{}^2}{3k^3T^3\ln(A/\dot{N})}\right]^{1/2} \tag{5}$$

This equation shows another necessary condition pertaining to the degree of supersaturation: To start the accumulation and the growth of the nuclei, the nucleation rate should be high enough to equilibrate or to surpass the redissolution rate of the particles. Taken together, S_c is the point at which the nucleation rate is so high that the number of nuclei increases even while smaller nuclei dissolve away.

However, the thermodynamic model discussed so far has some limitations with respect to nanocrystals. Whereas it is generally assumed that γ and ΔG_v are constant, these two values are strongly size-dependent for nanometer-sized particles.[10] As the particle size decreases, the ratio of surface atoms to the bulk atoms dramatically increases. As a result, there is a strong driving force, especially for nanocrystals with a size of few nanometers, to minimize the surface free energy

by reconstructing the surface structure or changing the crystal structure (e.g., through phase transitions[11] or lattice contraction[12]). The driving force to minimize the surface free energy also plays an important role in the formation of "magic number" metal clusters, which are composed of discrete numbers of metal atoms.[13] The occurrence of this "magic number" is attributed to the extra stability of the closed-shell structures.[13a,f] Molecular clusters also have discrete compositions with characteristic structures and are stable enough to be isolated and characterized. Homologous series of molecular clusters of CdSe and CdS have been reported.[14]

Although there is little knowledge about the identity of the nuclei generated during the synthesis of nanocrystals, the crystal embryos seem to be closely related to inorganic molecular clusters. In the case of CdSe nanocrystals, Peng and Peng reported that certain peaks in the absorption spectrum appeared repeatedly under various synthesis conditions.[6] They proposed that the crystal embryos are similar to CdSe molecular clusters on the basis of their similar absorption spectra. Zhanpeisov and co-workers calculated the molecular orbital energies for possible CdSe cluster structures and tried to correlate the calculated results with the experimentally observed absorption peak positions.[15]

2.1.2. *Synthetic Techniques for the Separation of Nucleation and Growth; Numerical Simulation of Burst Nucleation*

Both homogeneous and heterogeneous nucleation processes have been utilized to synthesize monodisperse nanocrystals by separating nucleation and growth. The seed-mediated growth method is the most apparent case for the separation of nucleation and growth, wherein nucleation is physically separated from growth by using preformed nanocrystals as seed nuclei. This method utilizes heterogeneous nucleation to suppress the formation of additional nuclei by homogeneous nucleation.[16] In this method, preformed nuclei are introduced into the reaction solution and then the monomers are supplied to precipitate on the surface of the existing nuclei. The monomer concentration is kept low during growth to suppress homogeneous nucleation. Seed-mediated growth is further divided into two categories: the synthesis of homogeneous particles[16a,c] and the production of heterogeneous structures, such as core/shell structures.[16b,d] There have been several reports on the fine size control of nanocrystals by separating nucleation and growth by the seed-mediated growth process.[16c,d] However, the seed particles need to be uniform to produce monodisperse nanocrystals.

There are two techniques that utilize homogeneous nucleation to synthesize monodisperse nanocrystals in the organic solutions: "hot-injection"[17] and "heating-up" methods.[18] The "hot-injection" technique was introduced by Bawendi and co-workers in their report on the synthesis of cadmium chalcogenide nanocrystals.[12a] This technique produces high degree of supersaturation by the rapid injection of excess precursor into a hot surfactant solution, resulting in burst nucleation by relieving the excess free energy of the supersaturation. During the nucleation process, the monomer concentration in the solution sharply decreases and thus nucleation rate slows down. This "hot-injection" method has been widely used to synthesize nanocrystals of metal chalcogenides,[12a,17a] transition metals,[17b] and noble metals.[17c] The heating-up method is a batch process in which the precursors, reagents, and solvent are mixed at a low temperature and heated up to a certain temperature to initiate the crystallization reaction. The heating-up method is particularly advantageous for large-scale production, because of its simplicity. Although this synthetic procedure is very simple, the size uniformity of the nanoparticles yielded by the heating-up method is often comparable to the best results obtained from the "hot-injection" method.[18a,b]

Characterizing the burst-nucleation process is challenging. Characteristic for this process is that there is a point of time at which the number of particles stops increasing and the particle concentration reaches a maximum. After this point, the reaction system enters the growth stage and the number of particles either remains constant or decreases. According to LaMer's model, the end of the nucleation stage is closely related to the decrease of the monomer concentration. Consequently, to prove the "burst-nucleation" model experimentally, both the particle concentration and the monomer concentration should be traced simultaneously.

Tracing the time evolution of the particle concentration and the monomer concentration is not a trivial task. For the heating-up method, the underlying mechanism for the formation of uniform nanoparticles has not yet been elucidated. Fortunately, in the synthesis of nanocrystals by the hot-injection technique, there have been several reports of the time evolution of the particle concentration of CdSe and ZnS nanocrystals.[19] These results were largely obtained from the optical properties of II–VI semiconductor nanocrystals, which have a distinct first excitonic peak in their absorption spectra originating from the quantum-confinement effect.[20] This peak is utilized to estimate the particle concentration and size distribution. The molar extinction coefficients at the first excitonic absorption peaks and their size dependences were measured experimentally for semiconductor nanocrystals of cadmium chalcogenides used as the reference data for determining the particle concentration.[21]

There are similar patterns in the reported data on the time evolution of the particle concentration (Figure 2): The nucleation stage, which is characterized by a rapid increase of the particle concentration, is very short or even not observable on the measurement timescale. At the end of the nucleation stage, the particle concentration reaches a maximum and then decreases slowly. Eventually, the concentration converges to a certain value. These observations are consistent with those expected for the separation of nucleation and growth. It seems that the crystallization processes of the hot-injection method (both nucleation and growth) start at stage II in the LaMer plot (Figure 1).[22]

To understand how the hot-injection method is used to achieve the separation of nucleation and growth, we simulated the homogeneous nucleation process by using a numerical method similar to that reported by De Smet et al.[23] Equation (4) is used to calculate the number of nuclei generated for each time step Δt. The radii of the newly generated nuclei are drawn from a normal distribution with a mean value of r_0 and relative standard deviation of 20%. New

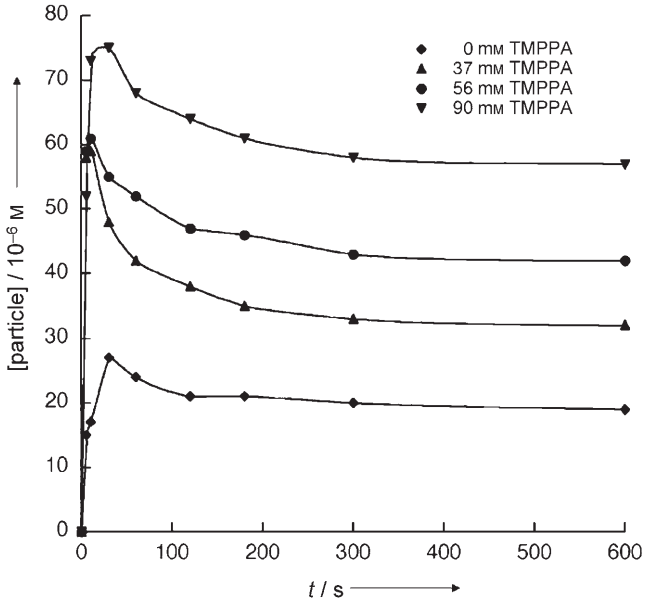

Figure 2. Experimental particle concentrations of CdSe nanocrystals as a function of time. CdSe nanocrystals were synthesized in binary ligand systems consisting of oleic acid (OLEA) and bis-(2,2,4-trimethylpentyl)phosphinic acid (TMPPA). Reaction solutions contained [Cd] = [Se] = 20 mM, [OLEA] = 225 mM. [TMPPA] was varied from 0 to 90 mM. The data are excerpted from reference [19d].

particles that are generated are included in the ensemble of particles. Individual particles in the ensemble can either grow or dissolve, depending on their sizes and reaction conditions. If a particle loses all of its monomers through dissolution, it is discarded from the ensemble and the total number of particles is reduced by one. The monomer concentration of the solution for each time step is calculated by subtracting the number of monomers present in particles at that instant from the total number of monomers. The values of parameters in the simulation model are selected or adjusted to fit the general synthetic conditions for CdSe nanocrystals. (For a more detailed description of the simulation, see reference [24].)

Figure 3a shows the simulated time evolution of the particle concentration and supersaturation during the first few seconds. In this simulation, the initial supersaturation is set high ($S = 100$) and the temperature is set to be constant. During the first two seconds, the particle concentration increases very rapidly, driven by the high supersaturation. The growth rate of these newly generated nuclei is also very high at such a high level of supersaturation. The nucleation and growth processes consume the monomers in solution so fast that the supersaturation of the solution rapidly falls. Consequently, the nucleation process effectively stops within the next second. Although most of the reaction rate parameters in this simulation, including the nucleation rate constant, diffusion rate constant, and growth rate constant, were set arbitrarily, the simulation result can explain qualitatively how hot injection works: The sudden induction of high supersaturation by the injection of precursors leads to the rapid consumption of the monomers and the subsequent rapid termination of the nucleation process, so that nucleation can be separated from growth.

There are three experimentally controllable parameters in Equation (4): supersaturation, temperature, and the surface free energy. Figure 3b shows the dependence of the time evolution of the particle concentration at various levels of initial supersaturation. As the initial supersaturation increases, the maximum particle concentration increases and the time required to reach the maximum decreases (Figure 3b inset). At the end of the nucleation stage, the supersaturation is too low for all the particles to keep growing. Particles smaller than r_c dissolve and the particle concentration declines slowly. The monomers that are formed from the dissolved particles diffuse toward larger particles and precipitate on them (this process, known as Ostwald ripening, is discussed in detail in the next section). The ensemble of particles in solution is in a pseudoequilibrium state, except that the monomers from smaller particles redistribute onto larger ones. As a result, the supersaturation is kept almost constant at a low level, and, consequently no additional

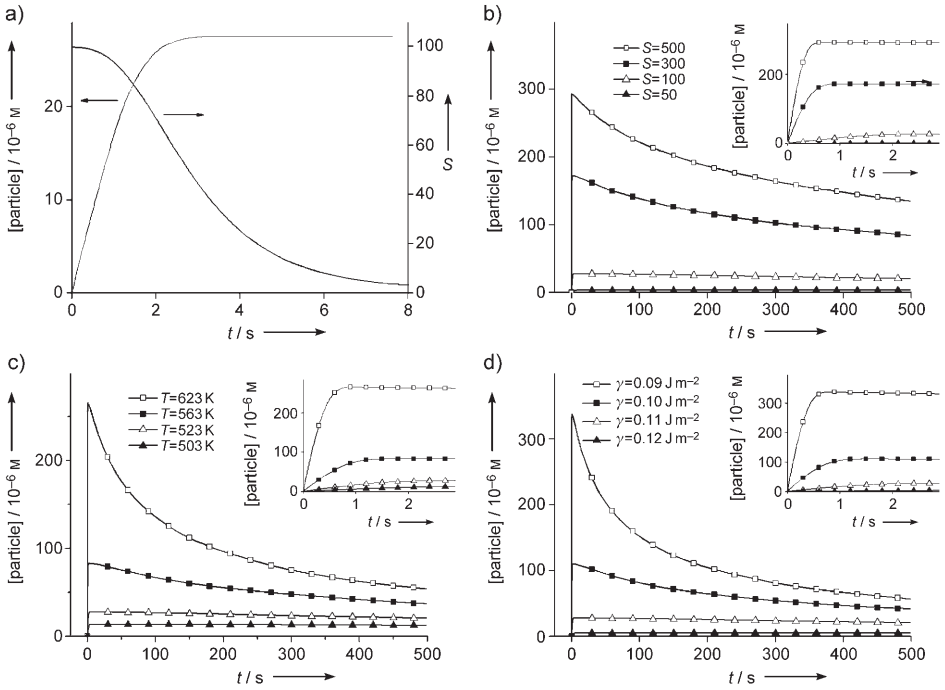

Figure 3. The results from numerical simulations of nucleation and growth of nanocrystals. a) The particle concentration and supersaturation as a function of time. Values of simulation parameters: $S = 100$, $T = 523$ K, $\gamma = 0.11$ J m^{-2}, $A = 10^7$ s^{-1}, $D = 10^{-15}$ m^2 s^{-1}, and $\Delta t = 10^{-2}$ s. b–d) Time evolution of the particle concentration for various degrees of supersaturation (b), temperatures (c), and surface free energies (d); the other simulation parameters are the same as in (a). Insets in (b–d) show expanded plots of the initial 3 s.

homogeneous nucleation can occur during the growth stage. The time evolutions of the particle concentration for various temperatures and surface free energy values were also simulated, and the results are shown in Figure 3c,d. Generally, the increase in temperature and decrease of the surface free energy exhibit similar trends to the increase of supersaturation. These simulation data reproduce the experimental result shown in Figure 2. This consistency strongly supports the validity of the theoretical model discussed so far.

2.2. Growth

In the previous section, we mentioned that the separation of nucleation and growth makes it possible to control the size distribution of an ensemble of particles. In this section, we show that growth without additional nucleation is a necessary condition for a narrow size distribution of the ensemble of particles.

The first theoretical studies on the narrowing of the size distribution during the growth process were performed by Reiss.[25] In his model, known as the "growth by diffusion" model, the growth rate of spherical particles depends solely on the flux of the monomers supplied to the particles (J). In this case, the relationship between the monomer flux and the growth rate dr/dt is given by Equation (6).

$$J = \frac{4\pi r^2}{V_m}\frac{dr}{dt} \tag{6}$$

If the average distance between the particles is large enough, then the diffusion layer formed at the periphery of each particle is undisturbed. Consequently, it is possible to treat each growing particle independently. For a single spherical particle in a homogeneous medium, there is concentration gradient around a particle with spherical symmetry. Fick's law [Eq. (7)] gives the flux J of monomers diffusing through the surface of a sphere enclosing the particle (D is the diffusion coefficient, C is the concentration, and $x(\geq r)$ is the distance from the center of the particle).

$$J = 4\pi x^2 D\frac{dC}{dx} \tag{7}$$

If J is assumed to be constant for x, the integration of $C(x)$ from r to $r+\delta$ with respect to x gives Equation (8).

$$J = 4\pi D\frac{r(r+\delta)}{\delta}[C(r+\delta)-C_s] \tag{8}$$

$C_s(=C(r))$ is the concentration at the surface of the particle. For sufficiently large values of δ ($r \ll \delta$), Equation (8) is reduced to Equation (9), in which C_{bulk} is the concentration of the bulk solution.

$$J = 4\pi r D(C_{bulk}-C_s) \tag{9}$$

Equation (10) follows from Equations (6) and (9).

$$\frac{dr}{dt} = \frac{V_m D}{r}(C_{bulk}-C_s) \tag{10}$$

If C_s and C_{bulk} are constant for all particles, the growth rate of a particle is inversely proportional to its radius. This result can be understood intuitively as follows: The number of monomers diffused onto the surface of a particle increases in proportion to the square of its radius, whereas the volume of a particle consisting of the monomers increases in proportion to the third power of its radius. Thus, the growth rate of a particle is decreased as the radius increases. With this result, it can be shown that for an ensemble of spherical particles, the variation of the radius distribution σ^2 is decreased during growth. From Equation (10), the value of σ^2 can be obtained as Equation (11), in which $\bar{r}$ and $\overline{(1/r)}$ are the mean values of r and $1/r$, respectively.

$$\frac{d(\sigma^2)}{dt} = 2V_m D(C_{bulk}-C_s)\left[1-\bar{r}\overline{\left(\frac{1}{r}\right)}\right] \tag{11}$$

Because the arithmetic mean differs from the harmonic mean, $\overline{(1/r)}$ is always greater than $1/\bar{r}$. Thus, for $C_{bulk} > C_s$, the right-hand side of Equation (11) is always negative. In other words, the variance of the size distribution of an ensemble of particles always decreases regardless of the initial size distribution as long as all of the particles are growing and no additional nucleation occurs. This is the self-regulating mechanism of the size distribution during the growth process and is often referred to as the "focusing" effect.[7]

However, the model described by Reiss is an oversimplification because it does not consider the reaction kinetics of crystal growth and its dependence on the particle size. As a result, the strong counter effect for the "focusing" mechanism is missing. During the growth process, there are two reactions acting in opposition to each other, namely, precipitation and dissolution [Eq. (12)].

$$n\,M^s \underset{k_d}{\overset{k_p}{\rightleftharpoons}} M_n^c \tag{12}$$

M^s and M^c refer to monomers in solution and in the crystal, and k_p and k_d are the reaction rate constants for precipitation and dissolution, respectively. It is assumed that the precipitation is the first-order reaction with respect to C_s[4a] and that the dissolution rate is independent of C_s. Then, at equilibrium $k_p C_{s,eq} = k_d$, which can be rewritten to give the surface concentration $C_{s,eq}$ [Eq. (13)].

$$C_{s,eq} = \frac{k_d}{k_p} \tag{13}$$

The change in chemical potential $\mu(r)$ of a spherical crystal with radius r with respect to that (μ°) of the bulk crystal arises from the surface free energy of area (A) [Eq. (14)].

$$\Delta\mu = \mu(r)-\mu^\circ = \gamma\frac{dA}{dn} \tag{14}$$

Because $dA = 8\pi r\,dr$ and $dn = 4\pi r^2\,dr/V_m$, Equation (14) can be rewritten as the Gibbs–Thomson relation Equation (15).

$$\Delta\mu = \frac{2\gamma V_m}{r} \tag{15}$$

The activated complex theory is adopted to assess the effect of the chemical potential change of a crystal on the precipitation and dissolution reactions. The variation of k_p and k_d with $\Delta\mu$ is given be Equations (16) and (17).

$$k_p = k_p^\circ \exp\left[-\alpha\frac{\Delta\mu}{RT}\right] = k_p^0 \exp\left[-\alpha\frac{2\gamma V_m}{rRT}\right] \tag{16}$$

$$k_d = k_d^\circ \exp\left[(1-\alpha)\frac{\Delta\mu}{RT}\right] = k_d^0 \exp\left[(1-\alpha)\frac{2\gamma V_m}{rRT}\right] \tag{17}$$

In these equations, α is the transfer coefficient and k^0 is the rate constant for the bulk crystal ($r=\infty$).[26a] Qualitatively, Equations (16) and (17) reveal that the smaller the radius of a particle is, the harder it is to grow but the easier it is to dissolve, because of its higher chemical potential. This is the effect is in contrast to the "focusing" mechanism, wherein smaller crystals grow faster. To combine this effect with the model of Reiss, the assumption that C_s is constant for all particles should be modified. The fluxes of the monomers toward the surface of a particle by precipitation and dissolution (J_p and J_d, respectively) for a particle with radius r are given by Equations (18) and (19).

$$J_p = 4\pi r^2 k_p^0 C_s \exp\left[-\alpha\frac{2\gamma V_m}{rRT}\right] \tag{18}$$

$$J_d = -4\pi r^2 k_d^0 \exp\left[(1-\alpha)\frac{2\gamma V_m}{rRT}\right] \tag{19}$$

The net flux J, then, is given by Equation (20), and the equation for C_s [Eq. (21)] is obtained by equating the expressions for J in Equations (9) and (20).

$$J = J_p + J_d = 4\pi r^2 k_p^\circ C_s \exp\left[-\alpha\frac{2\gamma V_m}{rRT}\right] - 4\pi r^2 k_d^\circ \exp\left[(1-\alpha)\frac{2\gamma V_m}{rRT}\right] \tag{20}$$

$$C_s = \frac{k_d^\circ r \exp\left[(1-\alpha)\frac{2\gamma V_m}{rRT}\right] + D\,C_{bulk}}{k_p^\circ \exp\left[-\alpha\frac{2\gamma V_m}{rRT}\right] + D} \tag{21}$$

Substituting this result into Equation (10) and using Equation (13) leads to Equation (22). $C_{s,eq}^\circ$ is the equilibrium surface concentration of the bulk crystal ($r\to\infty$), and S is the degree of supersaturation, which is defined as $S = C_{bulk}/C_{s,eq}^\circ$. This result can be rewritten in simplified form as Equation (23).[26a]

$$\frac{dr}{dt} = V_m D\,C_{s,eq}^\circ\left[\frac{S - \exp\left[\frac{2\gamma V_m}{rRT}\right]}{r + \frac{D}{k_p^\circ}\exp\left[\alpha\frac{2\gamma V_m}{rRT}\right]}\right] \tag{22}$$

$$\frac{dr^*}{d\tau} = \frac{S - \exp(1/r^*)}{r^* + K\exp(\alpha/r^*)} \tag{23}$$

The variables and parameters in Equation (23) can be normalized to dimensionless forms [Eqs. (24)–(26)].

$$r^* = \frac{RT}{2\gamma V_m} r \tag{24}$$

$$\tau = \frac{R^2 T^2 D\,C_{s,eq}^\circ}{4\gamma^2 V_m} t \tag{25}$$

$$K = \frac{RT}{2\gamma V_m}\frac{D}{k_p^\circ} \tag{26}$$

Equation (23) is a modified version of Equation (10) after both the mass transport and the reaction kinetics are considered. The growth rate of a single particle for various values of K and S are calculated from Equation (23) and plotted in Figure 4a, b.

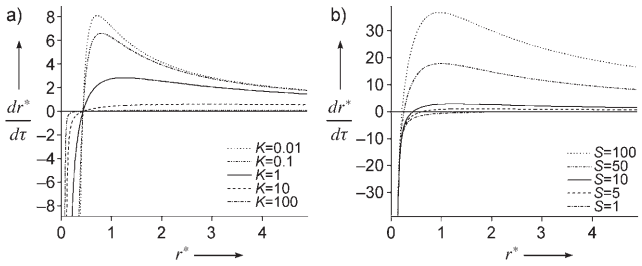

Figure 4. Growth rate as a function of radius calculated from Equation (23) for various values of K (a) and S (b). $\alpha = 0.5$, $S = 10$ in (a), and $K = 1$ in (b).

In Reiss' simple model, the "focusing" effect is derived by considering only mass-transport processes. However, the opposite effect comes from a kinetic process related to the Gibbs–Thomson effect. Figure 4a,b shows how these two effects compete with each other for the growth of an individual particle. A typical plot of growth rate for small values of K ($\ll 1$) and large values of S ($\gg 1$) has a maximum at $r^* = r^*_{max}$. For $r^* > r^*_{max}$, the size dependence of the crystal chemical potential is relatively small such that the variation of the growth rate with r^* mainly depends on mass-transport effects rather than on kinetic effects. Consequently, the slope of the graph is negative and a narrowing of the size distribution occurs in this region (the "focusing" region). In contrast, for $0 < r^* < r^*_{max}$, the situation is reversed. In this region, the crystal chemical potential is highly sensitive to the particle size. As r^* decreases, a particle becomes more unstable and the dissolution rate increases so fast that it dominates the net growth rate. As a result, larger particles have a higher growth rate and the slope of the graph is positive (the "defocusing" region). At $r^* = r^*_{zero}$ the growth rate is zero, and the rates of precipitation and dissolution are balanced. The value of r_{zero} can be obtained from Equations (23) and (24) [Eq. (27)].

$$r_{zero} = \frac{2\gamma V_m}{RT r^*_{zero}} = \frac{2\gamma V_m}{RT\ln S} \tag{27}$$

It is notable that this value is equal to r_c, which is evaluated by Equation (2) from the nucleation model. From

Figure 4, the factors affecting the evolution of the size distribution can also be deduced. In Equation (27), K represents the ratio of the rate of diffusion to the rate of the precipitation reaction. If the value of K is very small, the overall growth reaction rate is controlled by the diffusion rate, that is, the rate of mass transfer. This condition is called diffusion-controlled growth and is similar to the growth condition in Reiss' model. Consequently, the smaller the value of K is, the more effective the narrowing of the size distribution becomes. However, if the value of K is very large, the growth rate is mainly determined by the reaction rate. This condition is called reaction-controlled growth and the "focusing" effect is weakened under this condition. This trend is depicted in Figure 4a, which shows a steep negative slope for small values of K. An increase in the value of S always results in the enhancement of the growth rate according to Equation (23). However, the increment of the growth rate with S is decreased by a factor of $1/r^* + K\exp(\alpha/r^*)$ and thus is larger for smaller particles. In short, both the increase of S and the decrease of K enhance the "focusing" mechanism.

For an ensemble of particles, it is very difficult to trace the time evolution of the size distribution, mainly because C_{bulk} is not a constant but rather a function of the size of all the particles in the ensemble. Furthermore, the growth rates also depend on C_{bulk}. This mutual dependence makes it very difficult, if not impossible, to derive analytically the time evolution of the size distribution of the particles from Equation (23).

Talapin et al. presented another approach to solve this problem. They performed a numerical simulation of the time evolution of the particle size in an ensemble by using the Monte Carlo method (Figure 5).[26a] They used Equation (23) to calculate the growth rate for an individual particle. The initial size distributions of the ensembles of particles are set to normal distributions with various relative standard deviations and a mean value of $r_0 = 1$ nm. With these given ensembles of particles, simulations of the growth process were started with an initial supersaturation S_0. Figure 5a shows the time evolution of the size distribution of the particle ensemble. The initial reaction solution is highly supersaturated and the growth reaction operates under the diffusion-controlled condition. Two periods in the growth process can be distinguished in this figure. Initially ($0 < \tau < 10^{-2}$), the mean radius increases rapidly and the size distribution becomes narrower. In this period, the supersaturation is so high that r^*_{zero} is far below the mean radius $\langle r^* \rangle$ and, consequently, all of the particles are in the "focusing" region. In the second stage ($10^{-2} < \tau$), the growth rate declines sharply and the size distribution broadens. In this period, the supersaturation is low because of the rapid consumption of the monomer during the early period. As a result, the value of r^*_{zero} becomes comparable to that of $\langle r^* \rangle$ and many of the particles in the ensemble fall into the "defocusing" region (Figure 5b). Figure 5c depicts the relationship between the mean radius and the relative standard deviation of the size distribution for different initial supersaturations: A high initial supersaturation causes the "focusing" period to be maintained for a large mean radius, resulting in a low relative standard deviation at the end of the "focusing" period. Figure 5c also shows that

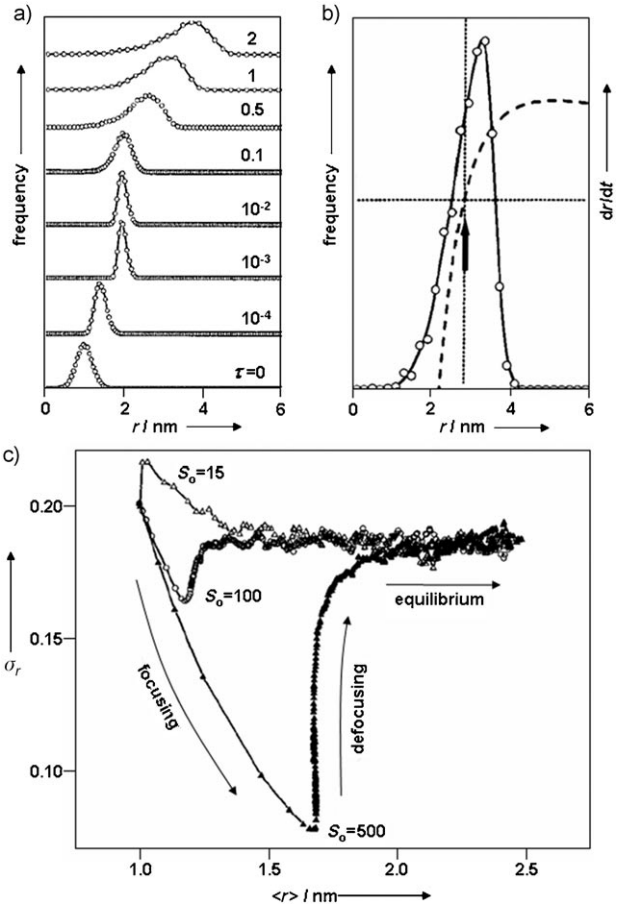

Figure 5. a) Time evolution of the size distribution of the ensemble of particles. b) The size distribution of particles (open circles and solid line) and the growth rate as a function of radius (dashed line) in the later period of the reaction. The arrow indicates the position of r_{zero}. c) Relative standard deviation versus mean radius for different initial levels of supersaturation. The data are excerpted from references [26a] and [26b].

the "defocusing" period leads to a similar equilibrium relative standard deviation regardless of the initial supersaturation. In the "defocusing" and equilibrium periods in which r_{zero} lies near $\langle r^* \rangle$, Ostwald ripening occurs. In this process, smaller particles dissolve and larger particles grow by receiving the monomers from the dissolving particles (This process was described in the previous section as an explanation for the decrease of the particle concentration during the growth stage). When the Ostwald ripening process is under pseudo-equilibrium state, the dissolving rate and reprecipitation rate of the monomers are balanced and the degree of supersaturation declines very slowly. Generally, the Ostwald ripening broadens the standard deviation of the particle size distribution. At the same time, the mean size of the particle ensemble is also increased. As a result, the relative standard deviation (the standard deviation divided by the mean value) converges to a certain value as the reaction system enters the pseudoequilibrium state. According to the simulation results by Talapin et al.,[26a] the relative standard deviation in the equilibrium period is almost independent of the initial size distribution but is lowered when the surface free energy is high.

The theoretical works discussed so far explain the behavior of the size distribution during the growth process when there is no additional nucleation. The theoretical studies[4,25,26] and simulations of Talapin et al.[26] reveal two underlying mechanisms for the control of the size distribution: 1) The "focusing" effect is a kinetically driven process that actively reduces the variance of the particle size distribution during the growth process. It works when the growth process is diffusion controlled and the degree of supersaturation is high. 2) Ostwald ripening occurs when the supersaturation is low.

In particular, in the pseudoequilibrium state, the relative standard deviation remains almost constant, whereas the mean size increases. This model has some limitations, however, because it considers the crystallization reaction merely as a solid–solute conversion. Many reactions involved in the synthesis of nanocrystals are more complicated. For example, sometimes the precipitation reaction and the dissolution reaction are not reversible.[27] In some cases, precursors do not seem to act directly as monomers, but instead undergo several intermediate reactions before the crystallization.

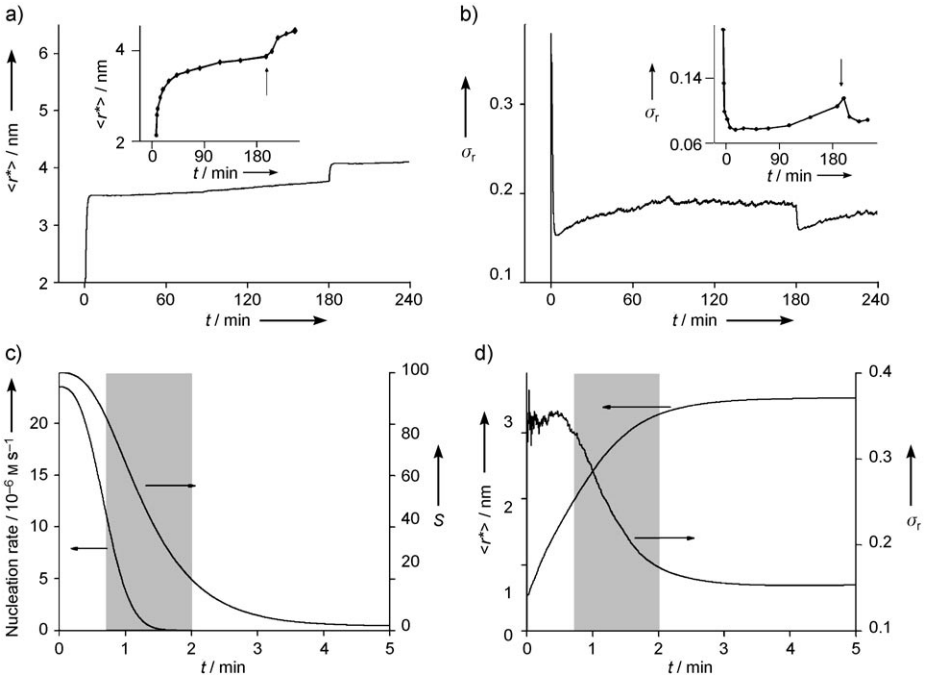

Figure 6. Results of a simulation of the CdSe nanocrystal synthesis by the hot-injection method and experimentally observed data excerpted from the reference [7]. Values of simulation parameters are the same as those in Figure 3a except for $A=3.7\times10^{5}\ s^{-1}$, $D=3.7\times10^{-17}\ m^{2}s^{-1}$, and $\Delta t=0.1$ s. The total amount of monomer was increased at 180 min by 24% of the initial value. a) Mean radius as a function of time. The inset shows the experimentally observed time evolution of mean size. b) The relative standard deviation as a function of time. The inset shows the experimentally observed time evolution of the relative standard deviation. The arrows in the insets of (a) and (b) indicate the point of time at which the additional monomers were injected. c) The nucleation rate and supersaturation versus time for the first 5 min. d) Mean radius and the relative standard deviation versus time for the first 5 min.

Experimental evidence for the "focusing effect" was provided by Alivisatos and co-workers, who reported that the size distribution of the semiconductor nanocrystals is strongly correlated to the degree of supersaturation.[7] They synthesized CdSe nanoparticles by the hot-injection method and traced the time evolution of the size and the size distribution of the nanocrystals by using photoluminescence (PL) spectroscopy. They observed that a fast increase of the mean particle size and a narrowing of the size distribution occurred simultaneously during the initial period of the growth process. In the later period, the growth rate decreased and the size distribution gradually broadened. The injection of additional monomers during this period resulted in the same effect as that observed during the initial period (insets of Figure 6a,b). This result confirms the relationship between the supersaturation level and the size "focusing" by growth and, consequently, support the "focusing" mechanism.

We attempted to reproduce the experimental results of Alivisatos and co-workers[7] by performing numerical simulations. We combined the "burst nucleation" model and the growth model represented by Equation (23), which were previously treated only separately, to show how these two mechanisms are correlated to achieve the monodispersity of the ensemble of the particles. We used the same simulation model introduced in the previous section but the simulation parameters were readjusted to imitate the experimental results. The additional injection during the later period of the reaction was simulated by increasing the total amount of the monomers by 24% at that time. As shown in Figure 6a,b, the result obtained from the simulation shows a good resemblance to the experimental results. With this simulation, we could trace the "focusing" effect in the earliest period of the hot-injection method. In Figure 6c, the nucleation rate and the degree of supersaturation are plotted for the first five minutes. The nucleation is almost complete after the first minute, but that the supersaturation level remains high during the next minute. Figure 6d clearly shows that it is during this second minute that the size distribution narrows rapidly, as during this period the necessary conditions for the focusing effect, namely, lack of nucleation and high supersaturation, are both satisfied. However, this situation cannot last for a long time because the level of supersaturation decreases very rapidly. After the "focusing" period, the reaction system undergoes Ostwald ripening.

The simulation results shown in Figure 6 demonstrate how "burst nucleation" and subsequent "focusing" are correlated. As mentioned in the previous section, the main purpose of "burst nucleation" is to terminate the nucleation reaction as soon as possible. Figure 6c shows that the early termination of nucleation leads to the widening of the window for the "focusing" effect (shaded areas in Figure 6c,d). If the nucleation process lasts until most of the monomers are consumed, this window will not exist. To enhance the "focusing" effect, it is desirable to widen the window between

the decrease of the nucleation rate and the decrease of the supersaturation, which can be experimentally achieved by the "burst-nucleation" process. Overall, the good resemblance between our simulations and the experimental results shown in Figure 6 clearly shows the validity of the theoretical model.

3. Various Chemical Synthetic Routes for Nanocrystals

Various physical and chemical methods have been used to synthesize nanocrystals. Physical methods such as metal evaporation, ball milling, and electrodeposition[28] have advantages in obtaining nanomaterials with high purity and are readily applicable to large-scale production. However, the size control and synthesis of monodisperse nanoparticles are very difficult with these physical methods.

The chemical methods are based on solution-phase colloidal chemistry. Uniform-sized nanoparticles with various sizes and shapes have been synthesized over the last ten years by using these chemical methods. In the following sections, three representative chemical methods are briefly discussed: reduction,[29,30] thermal decomposition,[31,32] and the nonhydrolytic sol–gel process.[27a,b] These three methods are classified on the basis of how the crystallization (both nucleation and growth) process occurs.

3.1. Reduction

Many reduction reactions, using various reductants such as sodium borohydride, hydrogen, and alcohols, have been used to synthesize metal nanoparticles. As early as 1853, Faraday reported the preparation of a colloidal gold sol (nanoparticles) from the reduction of $HAuCl_4$ with phosphorous.[33] Enustun and Turkevich synthesized a stable deep-red dispersion of uniform 13-nm gold nanoparticles by using sodium citrate as both a reductant and a stabilizer.[34] The reduction of metal salts with sodium borohydride has been extensively used to synthesize various metal nanoparticles.

Reverse micelles (surfactant-stabilized water-in-oil microemulsions) have been successfully used as nanoreactors for the synthesis of various nanoparticles. Klabunde and co-workers synthesized cobalt nanoparticles with sizes in the range from 1.8 to 4.4 nm by the reduction of a cobalt salt with $NaBH_4$ in reverse micelles formed using didodecyldimethylammonium bromide.[30b] Pileni and co-workers synthesized nanoparticles of various metals, including Co,[29c] Cu,[35] and Ag,[36] by the reduction of metal salts in reverse micelles.[37] However, there are several limitations for the synthesis of nanoparticles using reverse micelles.[38] Firstly, nanoparticles synthesized in reverse micelles are generally poorly crystalline, because the reactions are usually performed at low temperature. Secondly, the yield of the nanoparticles is often very low. Thirdly, polydisperse nanoparticles are often produced.

Organic-phase reduction reactions were performed using organic soluble reductants such as superhydride or alcohols to synthesize many metal nanoparticles. Bönnemann et al. cleverly utilized long-chain tetraalkylammonium salts of hydrotriorganoborate derivatives to generate nanoparticles of many transition metals. The long-chain tetraalkylammonium moiety functions as a surfactant to prevent the metal particles from agglomerating.[39] The Murray group at the IBM Watson Research Center synthesized Co nanoparticles by the reduction of a cobalt salt with superhydride ($LiBEt_3H$) at high temperature in the organic phase in the presence of surfactants such as oleic acid and trioctylphosphine (TOP).[27c] Many metallic nanoparticles, in particular of platinum group metals, have been synthesized by the reduction of metal salts with high boiling-point alcohols such as diols and ethylene glycol; this method is known as the polyol process.[40]

3.2. Thermal Decomposition Methods

The thermal decomposition reactions of organometallic compounds and metal–surfactant complexes were performed in hot surfactant solutions in the presence of surfactants to synthesize nanoparticles of various materials (Figure 7).

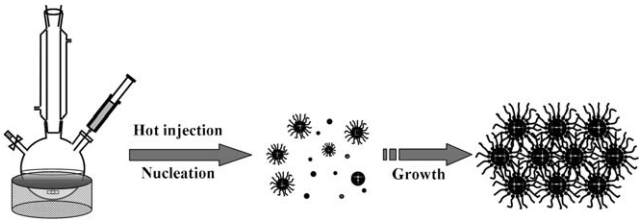

Figure 7. Hot-injection method for the synthesis of monodisperse nanoparticles.

Organic-phase synthetic methods have been widely used to synthesize nanoparticles because of their many advantages, such as the high crystallinity and monodispersity of the synthesized nanoparticles and their high dispersion ability in organic solvents.

The Bawendi group pioneered the thermal-decomposition method to synthesize monodisperse nanocrystals of cadmium chalcogenides.[12a] The rapid injection of organometallic precursors such as dimethyl cadmium and trioctylphosphine selenide into hot coordinating solvents induces a short burst of nucleation, and the subsequent growth by aging at slightly lower temperature generates CdSe nanocrystals. The effective separation of the nucleation and growth steps is the key to synthesizing monodisperse nanoparticles. The size of the nanocrystals could be tuned from 1.2 to 12 nm by varying the experimental conditions. The as-synthesized nanocrystals could be dispersed in organic solvents and they exhibited a quantum confinement effect. This pioneering work has been extended to the synthesis of nanocrystals of various materials such as semiconductors, metals, and metal oxides.

Organic-phase hot-injection synthetic methods based on fast nucleation in organic surfactants solutions often result in a size distribution with $\sigma \approx 10\,\%$, and a size-selection process is required to obtain monodisperse nanoparticles with a size distribution below 5%. This size-sorting process involves the

gradual addition of a hydrophilic solvent to the nanoparticles dispersion in a nonpolar solvent, which results in precipitation. The large nanoparticles first precipitate because of their strong van der Waals attraction. This size-selection process is very laborious and tedious.

3.3. Nonhydrolytic Sol–Gel Methods

The sol–gel process, which involves the hydrolysis and condensation of the precursors in acidic or basic aqueous alcohol media, is one of the most popular routes for the synthesis of oxide materials.[41a] However, the conventional sol–gel process has intrinsic limitations in the synthesis of nanocrystals in organic media: Firstly, sol–gel synthesis using H_2O molecules as an oxygen anion source is not compatible with the high temperature (>200 °C) colloidal synthetic route. Secondly, it is very difficult to form a homogeneous reaction solution, because the highly polar H_2O molecules are not miscible with organic solvents. Thirdly, the reaction rate of most metal precursors for oxide materials and H_2O is too fast to control the nanocrystal growth. In this regard, the nonhydrolytic sol–gel processes are excellent reaction pathways for metal oxide nanocrystals.

Vioux classified nonhydrolytic sol–gel reactions into nonhydrolytic hydroxylation reactions and aprotic condensation reactions, according to whether or not hydroxy groups are produced.[41b] The most well-known hydroxylation reaction is the thermal decomposition of metal alkoxides or carboxylates. In this process, hydroxy groups are produced on metal cations along with alkene side products through thermal decomposition. Although there have been several reports on the synthesis of metal oxide nanocrystals by the thermal decomposition of metal alkoxide or carboxylate precursors, a detailed mechanism was not given. The other hydroxylation route used for the synthesis of oxide nanocrystals is the reaction of a metal halide and an alcohol. The stabilization of the α-carbon atom by electron-donating groups facilitates this hydroxylation reaction (Scheme 1).

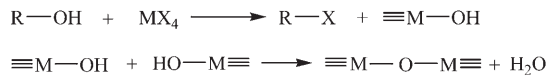

Scheme 1.

The two main reaction routes of aprotic condensation generally used in the synthesis of nanocrystals are the alkyl halide elimination and ester elimination reactions. In the case of alkyl halide elimination reaction, the reaction of metal halide and metal alkoxide produces a M-O-M linkage along with an alkyl halide by-product (Scheme 2). Similarly, in the ester elimination reaction, ester is produced as a by-product of the reaction of metal carboxylate and metal alkoxide (Scheme 3).

Because nonhydrolytic sol–gel reactions proceed by forming a μ-oxo bridge between two metal cations, the reactions are very useful for the synthesis of oxide nanocrystals with highly Lewis acidic (electron deficient) metal cations such as Ti^{4+}, Zr^{4+}, Hf^{4+}, and Sn^{4+}. Although these aprotic condensation reactions proceed at temperatures ranging from room temperature to around 100 °C, vacant sites on metal cations, which are essential to the formation of an oxide bridge between the metal ions, cannot be generated owing to the strong binding affinity of the coordinating surfactant at low temperature. Consequently, nonhydrolytic sol–gel reactions are generally performed at high temperatures (200–300 °C) so that the coordinating surfactants bind reversibly on the metal cations (Scheme 4).

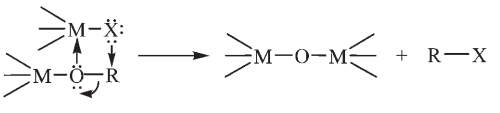

Scheme 2.

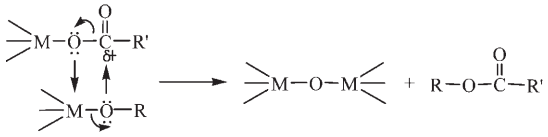

Scheme 3.

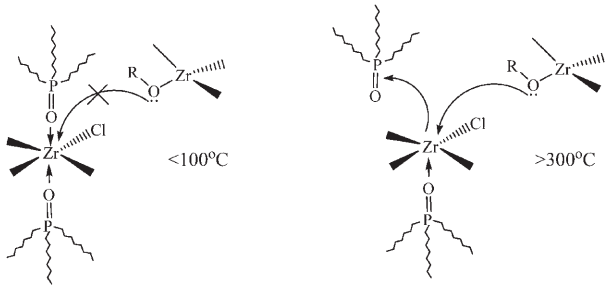

Scheme 4.

4. Monodisperse Nanocrystals of Metals and Their Oxides

4.1. Nanocrystals of Transition Metals and Their Oxides

Transition metals and metal oxides are one of the most fascinating classes of inorganic solids, since they exhibit a wide variety of structures, properties, and phenomena. In particular, many transition metals have been extensively used as catalysts for numerous industrial processes. Transition-metal oxides have been used in many important advanced technology areas, such as magnetic ferrites, ferroelectric oxides (barium strontium titanate (BST), lead zirconate titanate (PZT)), superconductors ($YBa_2Cu_3O_{7-x}$), ionic conductors (yittria-stabilized zirconia (YSZ)), phosphors using doped oxides, and photocatalysts (TiO_2). The syntheses of monodisperse nanocrystals of transition metals and metal oxides using various colloidal chemical routes are summarized in the following sections. The colloidal chemical synthesis of magnetic nanoparticles has been briefly reviewed by

Hyeon.[1e] The syntheses of monodisperse nanocrystals of metals and metal oxides are summarized in Table 1.

4.1.1. Co Nanocrystals

The group of Murray pioneered the synthesis of monodisperse nanocrystals of metallic magnetic materials.[42] They reported the synthesis of ε-phase cobalt nanocrystals by reduction of cobalt chloride in dioctyl ether at 200 °C in the presence of oleic acid and trialkylphosphine.[27c] The particle size was controlled by using alkylphosphines with various degrees of steric bulkiness. Short-chain alkylphosphines, such as tributylphosphine (TBP), permitted faster growth and resulted in larger particles (7–11 nm), whereas the bulky trioctylphosphine (TOP) produced smaller particles (2–6 nm). The size-selective precipitation by the gradual addition of ethanol to a hexane dispersion containing nanoparticles with various particle sizes produced cobalt nanocrystals with a narrow particle size distribution. These monodisperse cobalt nanoparticles were organized to form two- and three-dimensional superlattices, thus demonstrating the uniformity of the nanocrystals. The ε-phase cobalt nanocrystals were converted

Table 1: Synthesis of monodisperse nanocrystals of metals and their oxides.[a]

Materials	Precursors/Reagents	Surfactants	Solvents	Method[b]	Ref.
Co	$CoCl_2$/$LiBEt_3H$	OLEA, TOP	OE	R	[27c]
	$Co(AOT)_2$/$NaBH_4$	NaAOT	H_2O, isooctane	R	[44]
Fe	$[Fe(CO)_5]$	OLEA	OE	T	[32a]
	$[Fe\{N(SiMe_3)_2\}_2]$	$C_{16}NH_2$, OLEA, HDAC	mesitylene	T	[47]
FePt	$[Fe(CO)_5]$, $[Pt(acac)_2]$/HDD	OLEA, OAm, HDD	OE	T, R	[2a]
	$[Fe(CO)_5]$, $[Pt(acac)_2]$	OLEA, OAm	dibenzyl ether	T	[49]
	$[Fe(acac)_2]$, $[Pt(acac)_2]$/HDD	OLEA, OAm, HDD	OE	R	[50]
CoPt, $CoPt_3$	$[Co_2(CO)_8]$, $[Pt(acac)_2]$/HDD	ACA, $C_{16}NH_2$, HDD	PE, *o*-dichlorobenzene	T, R	[51]
	$[Co(CO)_3NO]$, $[Pt(acac)_2]$/HDD	OLEA, OAm, HDD	OE	T, R	[52]
FeCoPt	$[Fe(CO)_5]$, $[Pt(acac)_2]$, $[Co(acac)_2]$/HDD	OLEA, OAm, HDD	OE	T, R	[53]
γ-Fe_2O_3	$[FeCup_3]$	TOA		T	[55]
	$[Fe(CO)_5]$/trimethylamine *N*-oxide	OLEA	OE	T	[32a]
	$[Fe(CO)_5]$/air	OLEA	OE	T	[57]
	$[Fe(acac)_3]$/HDD	OLEA, OAm, HDD	PE	R	[61]
	$FeCl_3{\cdot}6H_2O$, $FeCl_3{\cdot}4H_2O$	OLEA	ODE	T	[65]
	FeO(OH)	OLEA	ODE	T	[18c]
	$FeCl_3{\cdot}6H_2O$, $Na(OLEA)_3$	OLEA	ODE	T	[18a]
$CoFe_2O_4$	$[(\eta^5\text{-}C_5H_5)CoFe_2(CO)_9]$	OLEA	OE	T	[58]
	$[Co(acac)_2]$, $[Fe(acac)_3]$/HDD	OLEA, OAm, HDD	PE	R	[62]
$MnFe_2O_4$	$[Mn_2(CO)_{10}]$, $[Fe(CO)_5]$	OLEA	OE	T	[59]
	$[Mn(acac)_2]$, $[Fe(acac)_3]$/HDD	OLEA, OAm, HDD	PE	R	[62]
	$[Mn(acac)_2]$, $[Fe(acac)_3]$/HDD	OLEA, OAm, HDD	dibenzyl ether	R	[63]
TiO_2	$Ti(OiPr)_4$, $Ti(OnBu)_4$	Me_4NOH	H_2O, isopropanol	S	[68]
	$TiCl_4$, $Ti(OiPr)_4$	TOPO	heptadecane	N	[27a]
$BaTiO_3$	$BaTi(O_2CC_7H_{15})[OCH(CH_3)_3]_5/H_2O_2$	OLEA	PE	S	[69]
ZrO_2	$Zr(OiPr)_4$, $ZrCl_4$	TOPO		N	[27b]
HfO_2, $Hf_xZr_{1-x}O_2$	$Hf[OCH(CH_3)_2]_4(CH_3)_2CHOH$, $HfCl_4$	TOPO		N	[70]
Cu_2O	$CuSO_4$/sodium ascorbate	CTAB	H_2O	R	[73]
	$[Cu(acac)_2]$	OAm		T	[74]
	$Cu(OAc)_2$	TOA, OLEA		T	[75]
MnO	$Mn(OAc)_2$	TOA, OLEA		T	[76]
	$[Mn(acac)_2]$	OAm, H_2O		T	[77]
	$[Mn_2(CO)_{10}]$	OAm, TOP		T	[32b]
Mn_3O_4	$Mn(HCOO)_2$	OAm		T	[78]
FeO	$[Fe(CO)_5]$, $Fe(OAc)_2$, $[Fe(acac)_3]$	TOA, OLEA	OE	T	[79]
Co_3O_4	$[Co(NO_3)_2{\cdot}6H_2O$, $C_6H_{13}OH$		octanol	T	[80]
Ni	$[Ni(acac)_2]$	OAm, TOP		T	[81]
Sn	$[Sn(NMe_2)_2]_2$/HCl	$C_{16}NH_2$	toluene	T	[83]
	$Sn(NMe_2)_2$	PS-*co*-PVP	diisopropylbenzene, THF	T	[16b]
In	InCp	PVP, TOPO	anisole, toluene	T	[84]
	InCp	PVP	THF	T	[16b]
In_2O_3	$[In(acac)_3]$	OAm		T	[18b]
	$In(OAc)_3$/trimethylamine *N*-oxide	OAm, OLEA	hexadecane	T	[85]
Bi	$Bi[N(SiMe_3)_2]_3$	PS-*co*-PVP	diisopropylbenzene, THF	T	[16b]
Gd_2O_3	$Gd(Ac)_3{\cdot}xH_2O$	OAm, OLEA	ODE	T	[86]
rare-earth oxide	Ln_2O_3,[c] $Ln(BA)_3(H_2O)_2$,	OAm, OLEA		T	[87]
CeO_2	$Ce(BA)_4$	OAm		T	[87]
CeO_2	$Ce(NO)_3$/PE	OAm, TOA		N	[88]

[a] For abbreviations, see the appendix at the end of this review. [b] T = thermal decomposition; R = reduction; N = nonhydrolytic sol–gel process; S = sol–gel process. [c] Ln = La, Pr, Nd, Sm, Eu, Gd, Tb, Er, Y.

into the thermodynamically stable hexagonal-close-packed (hcp) crystal form by annealing at 300 °C. The Alivisatos group also synthesized monodisperse ε-Co nanoparticles by rapid pyrolysis of dicobalt octacarbonyl ($[Co_2(CO)_8]$) in the presence of a surfactant mixture composed of oleic acid, lauric acid, and TOP.[43] They synthesized 3–17-nm-sized cobalt nanoparticles by varying experimental conditions such as the precursor/surfactant ratio, the reaction temperature, and the injection time.

Cobalt nanocrystals with other crystal structures were also synthesized by the Murray group. They synthesized hcp cobalt nanocrystals by the high-temperature reduction of cobalt acetate through a polyol process using 1,2-dodecanediol as both the reductant and the solvent in the presence of oleic acid and TOP.[42b] The particle size was tuned by varying the concentration or composition of the stabilizers. Increasing the concentration of oleic acid and TOP by a factor of two yielded smaller, 3–6-nm nanocrystals, whereas substituting TBP for TOP produced larger, 10–13-nm nanocrystals. Monodisperse nanocrystals were obtained by size-selective precipitation. A similar synthetic procedure was used to produce monodisperse nanocrystals of nickel and Co/Ni alloys. The Murray group also synthesized monodisperse multitwinned fcc cobalt nanocrystals by thermal decomposition of dicobalt octacarbonyl in the presence of a surfactant mixture composed of oleic acid and TBP at 200 °C and subsequent size-selective precipitation.

The Pileni group reported the synthesis of relatively uniform cobalt nanocrystals from the reaction between a micellar solution containing sodium bis(2-ethylhexyl)sulfosuccinate (NaAOT) and cobalt bis(2-ethylhexyl)sulfosuccinate ($Co(AOT)_2$), and sodium tetrahydroborate ($NaBH_4$, sodium borohydride) dissolved in a solution of NaAOT.[44] The as-synthesized nanoparticles were poorly crystalline, and after they were heated to 500 °C XRD revealed the characteristic pattern of fcc cobalt. A size-selection process involving the extraction of nanoparticles from a reverse micelle dispersion decreased the particle size from 6.4 to 5.8 nm, and the polydispersity was reduced drastically (from 21 to 11 %). The resulting uniform nanocrystals were self-assembled to generate a two-dimensional hexagonally ordered array.[45]

4.1.2. *Fe Nanocrystals*

Our research group synthesized monodisperse iron nanoparticles by thermal decomposition of an iron–oleate complex, which was prepared by treating iron pentacarbonyl ($[Fe(CO)_5]$) with oleic acid at around 100 °C.[32a] The particle size was controlled from 4 to 20 nm by varying experimental conditions such as the ratio of $[Fe(CO)_5]$ to oleic acid. The iron nanoparticles were poorly crystalline and were readily oxidized. Majetich and co-workers synthesized relatively uniform iron nanoparticles by thermal decomposition of $[Fe(CO)_5]$ with two methods.[46a] The first method involves a heterogeneous nucleation mechanism (seed-mediated growth), whereby platinum nanoclusters, synthesized from the polyol reduction of platinum(II) acetylacetonate ($[Pt(acac)_2]$), were used as nucleation seeds for the growth of the iron nanoparticles. The other method involves homogeneous nucleation from a supersaturated solution of $[Fe(CO)_5]$ and is thus quite similar to the synthesis of iron nanoparticles by our group. Iron nanoparticles with an average diameter ranging from 5 to 20 nm were produced by varying the reaction conditions and synthetic procedures. Very recently, Sun and co-workers synthesized iron nanoparticles stabilized with a Fe_3O_4 shell from a one-pot thermal decomposition of $[Fe(CO)_5]$ in the presence of oleylamine. The crystalline Fe_3O_4 shell generated from the controlled oxidation with trimethylamine *N*-oxide dramatically increased the chemical and dispersion stability of the nanoparticles.[46b] Chaudret and co-workers synthesized cube-shaped, monodisperse 7-nm iron nanocrystals by reduction of $[Fe\{N(SiMe_3)_2\}_2]$ with H_2 at 150 °C in the presence of hexadecylamine (HDA), oleic acid, and hexadecylamonium chloride.[47]

4.1.3. *Nanocrystals of Alloys of Fe and Co*

Monodisperse iron–platinum alloy nanocrystals were synthesized by the Murray group by reduction of $[Pt(acac)_2]$ using the polyol process with 1,2-hexadecanediol as a reductant and the thermal decomposition of $[Fe(CO)_5]$ in the presence of oleic acid and oleylamine.[2a] The composition of the alloy nanocrystals was varied by changing the molar ratio of the two precursors. The particle size could be controlled between 3 and 10 nm by adding more precursors to the previously synthesized 3-nm particles, which acted as seeds. Two- and three-dimensional superlattices were generated when the solvent was slowly evaporated. XRD revealed that the as-synthesized nanoparticles had a disordered face-centered-cubic (fcc) crystal structure and the nanoparticles transformed into a magnetically important face-centered-tetragonal (fct) structure when heated at 500 °C. A write/read experiment demonstrated that the annealed 120-nm-thick superlattice containing 4-nm $Fe_{48}Pt_{52}$ nanoparticles allowed magnetization reversals at moderate linear densities. Shevchenko et al. grew micrometer-sized colloidal FePt nanocrystals by using a three-layer technique based on the slow diffusion of a poor solvent into the bulk of a concentrated dispersion of nanocrystals through a buffer layer of a third component with a low, but not negligible, solubility for nanocrystals.[48a] Sun et al. used benzyl ether as the solvent and oleic acid and oleylamine as stabilizers for the one-pot synthesis of relatively uniform-sized FePt alloy nanocrystals from $[Fe(CO)_5]$ and $[Pt(acac)_2]$.[49] The size, composition, and shape of the nanocrystals were controlled by varying synthetic parameters such as the molar ratio of the stabilizers to metal precursor, the heating rate, and the temperature. Liu et al. synthesized monodisperse fcc FePt nanoparticles with an average size of 3 nm and a standard deviation approximately 10 % by the simultaneous reduction of $[Fe(acac)_2]$ and $[Pt(acac)_2]$ with 1,2-hexadecanediol as a reducing reagent in a polyol process.[50] Very recently, Varanda and Jafelicci, Jr. reported the synthesis of 4-nm-sized $Fe_{55}Pt_{45}$ nanoparticles from a mixture of iron(III) acetylacetonate and platinum acetylacetonate by a modified polyol process in refluxing 1,2-hexadecanediol. Annealing at 550 °C for 30 minutes converted the self-assembled fcc FePt alloy nanoparticles into

ferromagnetic fct nanocrystals with large coercivity.[48b] Recently, Sun reviewed the synthesis, self-assembly, and applications of monodisperse FePt nanoparticles.[48c]

Weller and co-workers reported the synthesis of monodisperse and highly crystalline $CoPt_3$ nanocrystals through a modified polyol process, whereby the nanocrystal size can be controlled only by a proper balance between the rates for nucleation and for growth from the molecular precursors.[51] Chen and Nikles synthesized nanocrystals of FePd and CoPt alloys by using a synthetic procedure similar to that used to synthesize FePt nanocrystals.[52] They synthesized 7-nm-sized $Co_{48}Pt_{52}$ nanocrystals by the simultaneous reduction of [Pt(acac)$_2$] and thermal decomposition of cobalt tricarbonylnitrosyl ([Co(CO)$_3$(NO)]) in the presence of oleic acid and oleylamine. They synthesized 11-nm-sized $Fe_{50}Pd_{50}$ nanocrystals by using a similar synthetic method with [Pd(acac)$_2$] and [Fe(CO)$_5$] as the precursors. They also synthesized $Fe_xCo_yPt_{100-x-y}$ nanocrystals by simultaneous reduction of [Co(acac)$_2$] and [Pt(acac)$_2$] and thermal decomposition of [Fe(CO)$_5$] in the presence of oleic acid and oleylamine.[53] Park and Cheon synthesized nanocrystals of solid Co/Pt solutions and Co/Pt core/shell structures by a redox transmetalation reaction between the reagents.[54] $CoPt_3$ alloy nanocrystals were generated by a reaction between [$Co_2(CO)_8$] and [Pt(hfac)$_2$] (hfac = hexafluoroacetylacetonate) in hot toluene. The reaction between [Pt(hfac)$_2$] with previously prepared 6.33-nm-sized Co nanoparticles produced a moderately monodisperse $Co_{core}Pt_{shell}$ nanocrystals with a particle size of 6.27 nm ($\sigma = 0.58$ nm), a Pt shell thickness of 1.82 nm, and a Co core size of 4.75 nm.[54a] They further extended this redox-transmetalation process to synthesize core/shell nanocrystals of Co@Au, Co@Pd, Co@Pt, and Co@Cu with particle sizes on the sub-10-nm scale.[54b]

4.1.4. *Ferrite Nanocrystals*

Nanocrystals of magnetic oxides, including most of the representative ferrites, have been studied for many years because of their many applications, such as magnetic storage media and as ferrofluids. However, the synthesis of monodisperse magnetic oxide nanocrystals has only recently been reported. The group of Alivisatos reported the synthesis of moderately monodisperse γ-Fe_2O_3 nanocrystals from the thermal decomposition of an iron Cupferron complex (Cup; *N*-nitrosophenylhydroxylamine, $C_6H_5N(NO)O^-$).[55] The particle size was controlled by varying either the reaction temperature or the amount of complex. Nanocrystals of Mn_3O_4 and Cu_2O were also synthesized from the corresponding metal Cupferron complexes.

Our group reported the direct synthesis of monodisperse, highly crystalline iron ferrite nanocrystals without a size-selection process.[32a] Figure 8 describes the overall synthetic procedure for the production of monodisperse ferrite nanocrystals. The monodisperse iron ferrite nanocrystals were produced by thermal decomposition of an iron–oleate complex, which was synthesized from [Fe(CO)$_5$] and oleic acid at 100 °C, followed by controlled chemical oxidation with trimethylamine *N*-oxide as a mild oxidant. In this synthesis, monodisperse but poorly crystalline iron nanoparticles were initially produced, and these were further oxidized to generate the desired iron ferrite nanocrystals. The particle size was controlled by varying the molar ratio of [Fe(CO)$_5$] to oleic acid. For example, monodisperse ferrite nanocrystals with particle sizes of 4, 8, and 11 nm were obtained by using reaction mixtures of [Fe(CO)$_5$] and oleic acid at molar ratios of 1:1, 1:2, and 1:3, respectively. Monodisperse 13-nm-sized ferrite nanocrystals were also synthesized by direct oxidative thermal decomposition of [Fe(CO)$_5$] in the presence of oleic acid and trimethylamine *N*-oxide. Recently, Masuda and co-workers used a two-dimensional hexagonal array of monodisperse 13-nm-sized magnetite nanocrystals as a template for the fabrication of highly ordered anodic porous alumina with a hole interval of 13 nm and a hole size of less than 10 nm; these are the smallest values thus far reported for anodic porous alumina with a highly ordered hole configuration.[56] Woo et al. synthesized uniform-sized magnetic iron oxide (maghemite or magnetite) nanocrystals with various particle sizes ranging from 5 to 11 nm by thermal decomposition of [Fe(CO)$_5$] in the presence of the residual oxygen in the system and by subsequent aeration.[57]

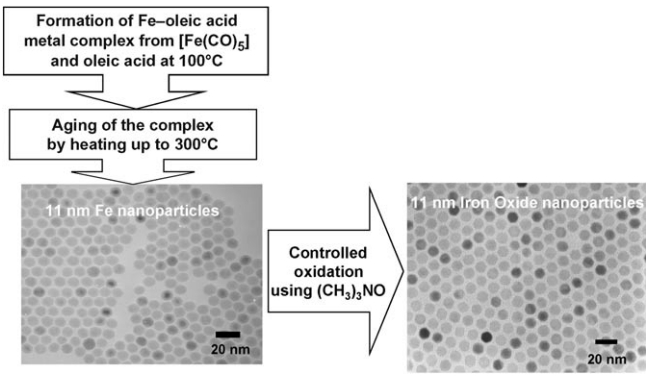

Figure 8. Direct synthesis of monodisperse, highly crystalline iron ferrite nanocrystals without a size-selection process.[32a]

Our group synthesized monodisperse nanocrystals of various ferrites by using a similar synthetic procedure involving the controlled thermal decomposition of a metal–surfactant complex and subsequent mild chemical oxidation. For example, [(η^5-C_5H_5)$CoFe_2(CO)_9$] was used as a single molecular precursor to synthesize cobalt ferrite ($CoFe_2O_4$) nanocrystals.[58] We also synthesized highly crystalline and monodisperse manganese ferrite ($MnFe_2O_4$) nanocrystals by thermal decomposition of metal–surfactant complexes prepared from [Fe(CO)$_5$], [$Mn_2(CO)_{10}$], and oleic acid, followed by mild chemical oxidation.[59] The particle sizes could be varied from 5 to 13 nm by altering the experimental parameters.

Markovich and co-workers synthesized magnetite (Fe_3O_4) nanocrystals by using the standard aqueous-precipitation technique, which involves a reaction between ammonium hydroxide and an aqueous solution containing $FeCl_3$ and $FeCl_2$ at a molar ratio of 2:1.[60] Monodisperse nanocrystals were obtained after several cycles of size-selective precipitation.

Sun and Zeng synthesized monodisperse iron ferrite nanocrystals by a high-temperature solution-phase reaction

of iron acetylacetonate with 1,2-hexadecanediol in the presence of oleic acid and oleylamine.[61] By using a similar synthetic procedure, Sun et al. synthesized monodisperse nanocrystals of $CoFe_2O_4$ and $MnFe_2O_4$ from a high-temperature reaction of $[Fe(acac)_3]$ and $[Co(acac)_2]$ or $[Mn(acac)_2]$ with 1,2-hexadecanediol.[62] The particle diameter was tuned from 3 to 20 nm by varying the reaction conditions or by seed-mediated growth. The hydrophobic nanocrystals were transformed into hydrophilic water-dispersable nanocrystals by mixing them with bipolar surfactants. Sun and co-workers also used a similar synthetic route to control the particle sizes of the $MnFe_2O_4$ nanocrystals by varying the precursor concentration and were able to synthesize uniform-sized cube-shaped $MnFe_2O_4$ nanocrystals by controlling the amount of stabilizers in the reaction mixture.[63] The group of Zhang obtained monodisperse spinel cobalt ferrite nanocrystals by combining a nonhydrolytic reaction with seed-mediated growth.[64] Spherical or cubic nanocrystals were formed depending on the growth rate.

Our group achieved a one-nanometer-level diameter controlled synthesis of monodisperse magnetic iron oxide nanocrystals synthesized by seed-mediated growth of previously synthesized monodisperse nanoparticle seeds.[16c] Monodisperse iron nanoparticles with sizes of 6, 7, 9, 10, 12, 13, and 15 nm could be synthesized by heating solutions of various combinations of 4-, 8-, or 11-nm iron nanoparticles with solutions of 1.5, 3.0, or 4.5 mmol iron–oleate complex. These synthesized iron nanoparticles were readily oxidized to iron oxide when exposed to air (Figure 9).

We reported the ultra-large-scale synthesis of monodisperse magnetite nanocrystals using inexpensive, nontoxic metal salts as reactants (Figure 10).[18a] Iron–oleate complex was prepared from hydrated iron chloride and sodium oleate rather than from toxic and expensive organometallic compounds such as $[Fe(CO)_5]$. The synthesized iron–oleate complex was added to an appropriate high-boiling-point

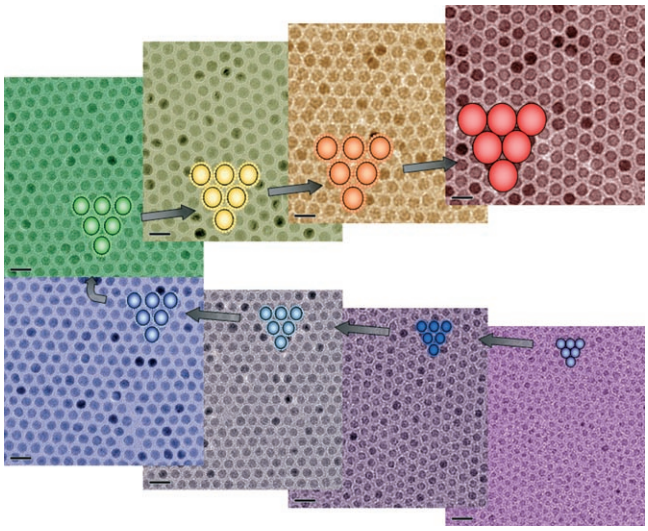

Figure 9. TEM images of iron oxide nanoparticles with particle diameters of 6, 7, 8, 9, 10, 11, 12, and 13 nm (clockwise from bottom right with 6 nm; scale bar: 20 nm); the diameter is controllable to one-nanometer accuracy.[16c]

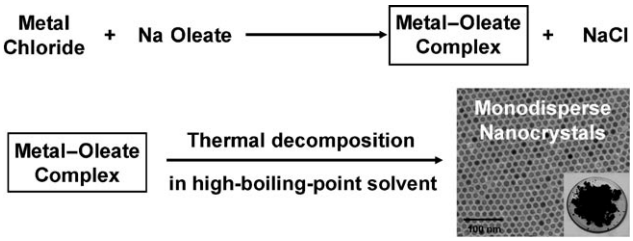

Figure 10. Overview of the ultra-large-scale synthesis of monodisperse nanocrystals. Metal–oleate precursors were prepared from metal chlorides and sodium oleate. Thermal decomposition of the metal–oleate precursors in high-boiling-point solvent produced monodisperse nanocrystals.[18a] TEM image of 12-nm magnetite nanocrystals synthesized in a 40 g quantity.

solvent, and slowly heated to around 300 °C to produce the nanocrystals. TEM image in Figure 10 shows 12-nm-sized magnetite nanocrystals that were synthesized in 40-g quantities. The particle size of the iron oxide nanocrystals could be controlled by using solvents with different boiling points. For example, 5-, 9-, 12-, 16-, and 22-nm-sized iron oxide nanocrystals were synthesized by using 1-hexadecene (bp 274 °C), octyl ether (bp 287 °C), 1-octadecene (bp 317 °C), 1-eicosene (bp 330 °C), and trioctylamine (bp 365 °C), respectively. The current synthetic procedure is quite general, and nanocrystals of many transition-metal oxides, such as MnO, CoO, and ZnO, have been synthesized by using a similar procedure.

Colvin and co-workers reported the synthesis of magnetite nanocrystals (6 to 30 nm) with narrow size distributions ($\sigma_r = 5$–$10\,\%$) by thermal decomposition of an iron–oleate complex prepared in situ from FeO(OH) and oleic acid in 1-octadecene.[18c] The group of Peng used a very similar synthetic procedure to synthesize monodisperse magnetite nanocrystals.[65] They prepared the iron–oleate complex by the reaction of $FeCl_3 \cdot 6\,H_2O$ or $FeCl_2 \cdot 4\,H_2O$ with oleic acid and subsequent neutralization of the HCl formed. The complex was dissolved in 1-octadecene and thermally decomposed at 300 °C to yield the monodisperse magnetite nanocrystals. Uniform-sized nanocrystals of transition-metal oxides such as Cr_2O_3, MnO, Co_3O_4, and NiO were produced by using a similar synthetic procedure involving the pyrolysis of metal–oleate complexes.

4.1.5. *Nanocrystals of TiO_2, ZrO_2, HfO_2, and ZnO*

Titania (TiO_2) is an n-type semiconductor material with a large indirect band gap (3.2 eV). It has been used in dye-sensitized solar cells (DSSCs), photocatalysts, and photochromic devices.[66] TiO_2 nanocrystals have been synthesized by various methods, including reactions in reverse micelles, polyol reactions, sonochemical synthesis, and sol–gel reactions.[67] To synthesize uniform-sized TiO_2 nanocrystals, control of the reactivity of the titanium precursors, such as titanium(IV) chloride ($TiCl_4$) and titanium alkoxides ($Ti(OR)_4$), is critical on account of the high reactivity of the precursors. Chemseddine and co-workers synthesized uniform-sized anatase TiO_2 nanocrystals with different sizes and shapes by hydrolysis and polycondensation of titanium alkoxides such as titanium(IV) isopropoxide ($Ti(O\mathit{i}Pr)_4$) and

butoxide ($Ti(OnBu)_4$) in the presence of tetramethylammonium hydroxide (Me_4NOH).[68] Tetramethylammonium hydroxide not only catalyzed the reaction as a base catalyst but also provided an organic cation to stabilize the anatase nanocrystals. The size and shape of the anatase nanocrystals were controlled by adjusting the relative concentrations of titanium alkoxide and Me_4NOH, the reaction temperature, and the pressure. However, the disadvantage of this synthetic procedure is the low yield as a result of the low concentration of the reaction mixture.

O'Brien et al. synthesized uniform-sized barium titanate (BTO) nanocrystals from barium titanium (ethylhexano)isopropoxide ($BaTi(O_2CC_7H_{15})[OCH(CH_3)_2]_5$) and hydrogen peroxide at 100 °C in the presence of diphenyl ether and oleic acid.[69] The particle size varied from 6 to 12 nm depending on the molar ratio of the precursor and oleic acid.

Recently, nonhydrolytic sol–gel processes have been used to synthesize various transition-metal-oxide nanocrystals. In contrast to sol–gel methods, which are based on the hydrolysis and condensation of metal precursors in aqueous alcohol, nonhydrolytic sol–gel reactions proceed by a reaction between the metal precursors in organic media (Scheme 5).[41b] Colvin and co-workers reported the synthesis

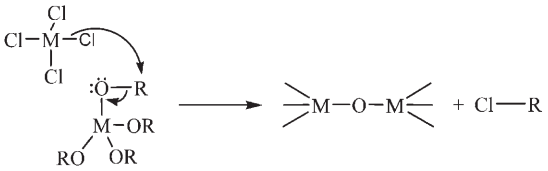

Scheme 5.

of titania nanocrystals by a nonhydrolytic sol–gel reaction between titanium(IV) chloride and titanium(IV) isopropoxide with liberation of isopropyl chloride as the by-product (alkyl halide elimination).[27a] In this synthesis, trioctylphosphine oxide (TOPO) was used as the coordinating ligand for the titania nanocrystals. Despite the polydispersity of the titania nanocrystals produced, they showed that a nonhydrolytic sol–gel reaction could be applied to the synthesis of metal oxide nanocrystals in the absence of H_2O.

Our research group employed a similar procedure to produce uniform-sized ZrO_2 nanocrystals.[27b] A nonhydrolytic sol–gel reaction between zirconium(IV) isopropoxide ($Zr(OiPr)_4$) and zirconium(IV) chloride ($ZrCl_4$) at 340 °C generated monodisperse tetragonal zirconia nanocrystals with a particle size of 4 nm (Figure 11). Zirconia nanocrystals with an average size of 2.9 nm were obtained when zirconium(IV) bromide ($ZrBr_4$) was used as the precursor instead of zirconium(IV) chloride. Under optimized synthetic conditions, we could synthesize as much as 5 g of nanocrystals by using 20 mmol (7.8 g) of zirconium(IV) isopropoxide and 25 mmol (5.83 g) of zirconium(IV) chloride. Brus and coworkers further extended these synthetic methods to produce uniform-sized HfO_2 and $Hf_xZr_{1-x}O_2$ nanocrystals.[70] ZnO nanocrystals were also synthesized through nonhydrolytic sol–gel route based on the ester elimination reaction between zinc acetate and alcohol (Scheme 6). In this reaction, an

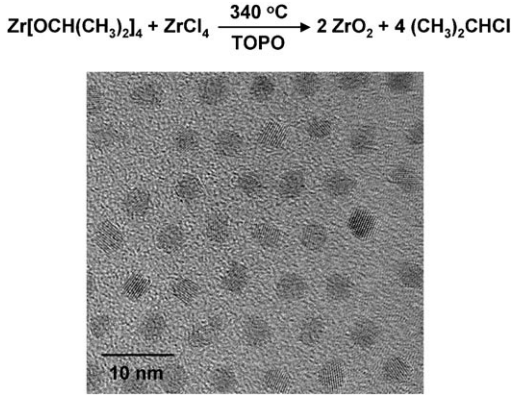

Figure 11. Monodisperse tetragonal zirconia nanocrystals with a particle diameter of 4 nm.[27b]

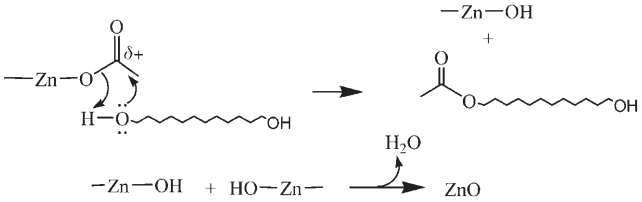

Scheme 6.

electron pair on the oxygen atom of the alcohol attacks an electron-deficient carbonyl carbon center of the acetate.[71]

Kahn, Chaudret, and co-workers synthesized monodisperse 3.5-nm-sized ZnO nanocrystals by slow hydrolysis in air of a solution of bis(cyclohexyl)zinc ($ZnCy_2$) in THF with one equivalent of a long-alkyl-chain amine and half an equivalent of a long-alkyl-chain acid. These nanoparticles spontaneously organize into 2D and 3D superlattices, thus demonstrating their good size uniformity.[72]

4.1.6. Nanocrystals of Cu and Cu_2O

Gou and Murphy synthesized monodisperse cube-shaped Cu_2O nanoparticles by reduction of $CuSO_4$ with sodium ascorbate as a reducing agent in the presence of a cetyltrimethylammonium bromide (CTAB) surfactant.[73] The surfactant concentration was used to control the average edge length of the cubes from 200 to 450 nm. TEM showed that these nanocubes were composed of small nanoparticles, which appeared to be hollow. Our group synthesized uniform copper nanoparticles with a diameter of 15 nm by thermal decomposition of $[Cu(acac)_2]$ in oleylamine.[74] Subsequent air oxidation generated Cu_2O-coated Cu nanoparticles. The nanoparticles were used as an active catalyst for Ullmann-type amination reactions with various aryl chlorides, whereas commercial micrometer-sized copper particles are active only for more expensive aryl bromides. Recently, O'Brien and coworkers synthesized monodisperse Cu_2O nanocrystals by thermal decomposition of copper(I) acetate ($Cu(Ac)_2$) in a solution of trioctylamine and oleic acid.[75] The diameters of the Cu_2O nanocrystals could be tuned from 3.6 to 10.7 nm by controlling the molar ratio of oleic acid and copper acetate.

4.1.7. Manganese Oxide Nanocrystals

Yin and O'Brien synthesized monodisperse 7-nm MnO nanocrystals by thermal decomposition of manganese acetate in the presence of oleic acid at 320 °C.[76] MnO nanocrystals with average diameters of 12, 14, 18, and 20 nm were synthesized by aging at 100 °C for 5, 10, 30, and 60 min, respectively, after heating at 320 °C for 1 h. The group of Park synthesized monodisperse 10-nm Mn_3O_4 nanocrystals by thermal decomposition of manganese acetate in oleylamine at 180 °C for 9 h in an argon atmosphere.[77] The particle size could be varied easily by changing the reaction temperature. For example, 6-nm-sized nanocrystals were obtained at 150 °C, and 15-nm-sized nanocrystals were prepared at 250 °C. Cubic MnO nanocrystals were produced when 10 equivalents of water was introduced to the reaction slurry containing manganese acetate in oleylamine (1:24 molar ratio). By changing the reaction temperature, MnO nanocrystals with sizes of 11 nm (220 °C, 9 h), 17 nm (220 °C, 3 h and then 250 °C, 6 h), and 22 nm (250 °C, 9 h) were synthesized. The authors claimed that the presence of water prohibited further oxidation of the synthesized MnO, presumably because the water was involved in the decomposition of the acetylacetonate ligand, which acts as the oxygen source. Our group synthesized monodisperse 5-nm-sized MnO nanocrystals by thermal decomposition of an Mn–oleylamine complex in TOP at 300 °C.[32b] The particle sizes of the nanocrystals were controlled from 5 to 40 nm by changing the surfactant. Ten-nanometer-sized MnO nanoparticles were produced when triphenylphosphine was used instead of TOP. Aging the reaction mixture prepared in TOP for 2 days at 100 °C resulted in the formation of 40-nm-sized monodisperse MnO nanoparticles. Detailed structural characterization by XRD and X-ray absorption spectroscopy showed that the nanoparticles had core/shell structures with a thin Mn_3O_4 shell.

Zhang, Yan, and co-workers synthesized monodisperse nanocrystals of Mn_3O_4, CoO, and CuOx in large quantities by thermolysis of the corresponding metal–formate precursors in oleylamine/oleic acid.[78] The size of the nanocrystals can be easily manipulated by changing the synthetic parameters.

4.1.8. FeO Nanocrystals

Redl et al. reported the detailed structural, magnetic, and electronic characterization of nonstoichiometric iron oxide (wüstite) nanocrystals prepared by decomposition of iron(II) and iron(0) precursors in the presence of organic solvents and capping groups.[79]

4.1.9. Co_3O_4 Nanocrystals

Chen and co-workers synthesized monodisperse 5-nm Co_3O_4 nanocrystals by thermal decomposition of $Co(NO_3)_2{\cdot}7\,C_6H_{13}OH$, which was prepared from cobalt nitrate ($Co(NO_3)_2{\cdot}6\,H_2O$) and *n*-hexanol.[80] Controlled aging of the nanoparticle solution after addition of an appropriate amount of water caused the aggregation of the primary 5-nm-sized nanocrystals to generate a spherical mesoporous-like nanostructure with diameters ranging from 40 to 200 nm.

4.1.10. Nanocrystals of Ni and NiO

Our group synthesized monodisperse Ni nanoparticles by thermal decomposition of an Ni–oleylamine complex (prepared from $[Ni(acac)_2]$ and oleylamine) in a hot phosphine solvent.[81a] The size of the nickel nanoparticles was controlled by varying the type of phosphines that were used both as the solvent and the surfactant. The bulky TOP limited the growth of the particles, which led to the formation of 2-nm-sized particles. The less bulky TBP and triphenylphosphine resulted in the production of 5- and 7-nm-sized spherical nanoparticles, respectively. The self-assembly of the synthesized nanoparticles by controlled evaporation of the solvent yielded Ni nanocrystal superlattices. X-ray absorption spectroscopy, magnetic circular dichroism, and magnetic measurement showed that the nanoparticles were readily oxidized to NiO nanoparticles. Very recently, we used partially oxidized Ni/NiO core/shell nanoparticles for the separation of histidine-tagged proteins.[81b]

4.1.11. Cr Nanocrystals

Uniform-sized chromium nanoparticles were synthesized by thermal decomposition of a Cr–TOP complex prepared from a chromium carbene complex and TOP.[82] Cr nanoparticles with sizes ranging from 2.5 to 6 nm were synthesized by adding various amount of dioctyl ether into the reaction mixture. The synthesized Cr nanoparticles were quite sensitive to air and readily oxidized to Cr_2O_3 upon exposure to air.

4.2. Nanocrystals of Main-Group Metals and Their Oxides

Chaudret and co-workers synthesized monodisperse nanocrystals of various metals from corresponding organometallic compounds. Tin nanoparticles ($18 \times 15\ nm^2$) were synthesized by UV irradiation (365 nm) of $[\{Sn(NMe_2)_2\}_2]$ in toluene at room temperature without stirring in the presence of a mixture of hexadecylamine and its HCl adduct (HDA·HCl).[83] The monodisperse Sn nanoparticles were self-organized to generate the superlattice structures (Figure 12).

Monodisperse amorphous indium nanoparticles with a diameter of 5.2 nm were synthesized from $[In(\eta^5\text{-}C_5H_5)]$ (InCp) and TOPO at room temperature or 50 °C in toluene containing approximately 50 ppm H_2O.[84] These monodisperse In nanoparticles were assembled to generate superlattice structures. Some of the nanoparticles were oxidized to form In_2O_3 nanoparticles. The Park group synthesized monodisperse In_2O_3 nanocrystals by thermal decomposition of indium acetylacetonate in oleylamine.[18b] In_2O_3 nanocrystals with particle sizes ranging from 4 to 8 nm were synthesized by either varying the precursor/surfactant ratio or by a multiple injection of the precursor. These In_2O_3 nanocrystals were sufficiently uniform to self-assemble into superlattice structures. Fang and co-workers synthesized

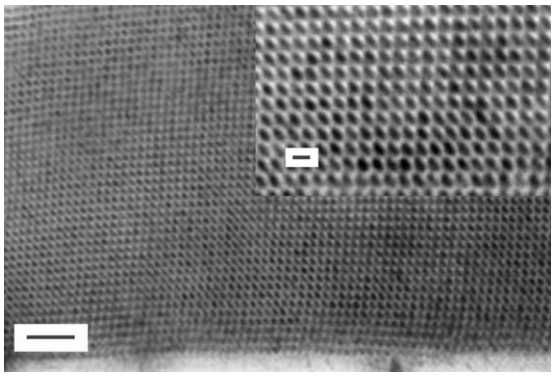

Figure 12. Superlattice structure of self-assembled monodisperse Sn nanoparticles (scale bar: 100 nm). Inset: higher magnification (scale bar: 20 nm).[83]

monodisperse In_2O_3 nanocrystals from indium acetate and trimethylamine *N*-oxide in hexadecane in the presence of oleylamine and oleic acid at 290 °C.[85] Monodisperse In_2O_3 nanocrystals with uniform particle sizes ranging from 11.5 to 20.0 nm were synthesized by a dynamic-injection method, which involved the addition of an as-prepared reaction mixture into a similar reaction mixture heated to 290 °C with subsequent aging. The overall process is similar to seed-mediated growth.

Buhro and co-workers reported the synthesis of monodisperse nanoparticles of Bi, Sn, and In by seed-mediated growth using Au nanoclusters as seeds.[16b] They used $Au_{101}(PPh_3)_{21}Cl_{15}$ clusters, which have a 1.5-nm-diameter Au core, as the seeds. The $Bi[N(SiMe_3)_2]_3$ and $Sn(NMe_2)_2$ precursors were thermally decomposed at 150 and 140 °C, respectively, in the presence of poly(styrene$_{0.86}$-*co*-vinylpyrrolidinone$_{0.14}$). The In precursor InCp was decomposed at room temperature by adding methanol in the presence of poly(vinylpyrrolidinone). The uniform particle sizes of the nanocrystals ranged from 7 to 25 nm depending on the concentration of Au nanocluster seeds and the metal precursor.

4.3. Nanocrystals of Lanthanide Oxides

Cao reported the synthesis of uniform-sized Gd_2O_3 nanoplates with an edge length of 8.1 nm and a thickness of as low as 1.1 nm by thermolysis of gadolinium acetate hydrate dissolved in a solution of oleylamine, oleic acid, and octadecene.[86] Yan and co-workers synthesized nanocrystals of ceria and other rare-earth oxides with various shapes by thermolysis of metal benzoylacetonate complexes in a mixture of oleic acid and oleylamine.[87] In particular, monodisperse 2.6-nm CeO_2 nanocrystals were synthesized. Our group synthesized spherical ceria nanocrystals with diameters of 3.5 and 5.2 nm from cerium(III) nitrate ($Ce(NO)_3$) and phenyl ether at 320 °C in the presence of oleylamine and a mixture of oleylamine and trioctylamine, respectively.[88]

5. Semiconductor Nanocrystals

Colloidal semiconductor nanocrystals, in particular metal chalcogenide nanocrystals, have attracted a great deal of attention on account of their quantum confinement effects and size-dependent photoemission characteristics.[12b,20,89] These semiconductor nanocrystals, also known as quantum dots, have been used in many different technological areas, including biological labeling and diagnostics, light emitting diodes, electroluminescent devices, photovoltaic devices, lasers, and single-electron transistors.[90] Semiconductor nanocrystals with different sizes and shapes have been synthesized by various solution-phase synthetic schemes including the most popular organometallic synthetic procedure involving high-temperature thermolysis of precursors. Reports of syntheses of monodisperse semiconductor nanocrystals are summarized in Table 2.

5.1. Nanocrystals of Chalcogenides of Cadmium and Zinc

The Bawendi group pioneered the synthesis of monodisperse CdSe nanocrystals. In 1993, they reported the synthesis of CdE (E = S, Se, Te) nanocrystals by a hot-injection method whereby a cold TOP solution containing the metal and chalcogenide precursors was rapidly introduced into hot TOPO solution.[12a] Nuclei of the CdE nanocrystals formed immediately, and this was followed by growth at a lower temperature without further nucleation. Relatively uniform CdSe nanocrystals with a particle size distribution of $\sigma_r = 10\,\%$ could be produced by separating the nucleation and growth stages with this hot-injection process. Further size-selection processes produced monodisperse nanocrystals with a narrow size distribution of $\sigma_r = 5\,\%$.

As mentioned above, monodisperse nanocrystals can be obtained not only by the kinetic control of the reaction conditions, such as the growth time, temperature, and monomer concentration, but also by the choice of proper coordinating surfactants, which prevent the agglomeration of nanocrystals and controls their growth rate. Weller and co-workers presented a good example of the synthesis of uniform-sized CdSe nanocrystals with a size distribution of 4 % under ligand control by adding hexadecylamine to the TOP-TOPO solution,[17a] as first developed by Bawendi and co-workers.[12a] Figure 13 shows TEM and HRTEM images of three-dimensional superlattices of monodisperse CdSe nanocrystals.[1c] Under these synthetic conditions, nanocrystals grew without a defocusing process. Hines and Guyot-Sionnest noted that the intermediate binding ability of the primary amine to Zn cations, which lies between TOPO and TOP, led to the growth of ZnS nanocrystals with a narrow size distribution.[91] Moreover, the less sterically hindered primary amine forms a denser coordination layer on the nanocrystals surface than the highly hindered trialkylphosphine compounds, which improves the stability of the nanocrystal surface and optical properties.

Peng and co-workers synthesized CdSe nanocrystals with narrow size distributions by using either cadmium oxide (CdO) or cadmium acetate ($Cd(Ac)_2$) as a precursor instead

Table 2: Synthesis of monodisperse semiconductor nanocrystals.

Materials	Precursors/Reagents	Surfactants	Solvents	Method[a]	Ref.
CdS	Me_2Cd, $(TMS)_2S$			T	[12a]
CdSe	Se, $(TMS)_2Se$	TOP, TOPO		T	[12a]
CdTe	Te, $(BDMS)_2Te$			T	[12a]
CdSe	Me_2Cd, Se	TBP, TOPO		T	[7]
InAs	$(TMS)_3As$, $InCl_3$	TOP		T	[7]
CdSe	Me_2Cd, Se	TOP, TOPO		T	[26b]
CdTe	$Cd(ClO_4)_2$, Al_2Te_3	thioglycolic acid		L	[26b]
InAs	$InCl_3$, $(TMS)_3As$	TOP		T	[26b]
CdSe	$Cd(Ac)_2$, $CdCO_3$, CdO, Se	TOPO, SA, LA, TDPA, $C_{12}NH_2$, TOP		T	[92b]
CdSe/ZnS	Me_2Cd, Se, Et_2Zn, $(TMS)_2S$	TOPO, TOP, $C_{16}NH_2$		T	[17a]
CdSe/CdS	$Cd(Ac)_2$, Se, H_2S	$C_{16}NH_2$, TOPO, TOP, TDPA		T	[93]
	CdO, Se, TBP, OLEA	SA, $C_{18}NH_2$, TOPO	ODE	T	[99]
CdS	CdO, S	OLEA	ODE	T	[92c]
	cadmium xanthate	$C_{16}NH_2$		T	[97]
CdTe	CdO, Te	TOPO, TOP, TDPA		T	[92a]
ZnSe	Et_2Zn, Se	TOP, $C_{16}NH_2$		T	[91]
ZnSe, ZnS	$Zn(SA)_2$, Se, S	$C_{18}NH_2$, TBP, SA	tetracosane, ODE	T	[96e]
PbS, ZnS, CdS, MnS	$PbCl_2$, $ZnCl_2$, $CdCl_2$, $MnCl_2$, S	OAm		L	[18d]
ZnS	Et_2Zn, S	$C_{16}NH_2$, OAm, OLEA	ODE	T	[103]
PbSe	$Pb(Ac)_2{\cdot}3\,H_2O$, Se	OLEA, TOP	PE	T	[96a]
	$Pb(Ac)_2{\cdot}3\,H_2O$, Se	OLEA, TOP	PE	T	[96c]
	PbO, Se	OLEA, TOP	ODE	T	[96d]
	$Pb(Ac)_2{\cdot}3\,H_2O$, Se	OLEA, TOP	PE	T	[105]
	$Pb(OLEA)_2$, Se	TOP	PE	T	[42a]
PbTe	$Pb(Ac)_2{\cdot}3\,H_2O$, Te	OLEA, TOP	PE	T	[96b]
Cu_2S	copper thiolate			T	[108, 109]

[a] T = thermal decomposition; L = Lewis acid–base reaction.

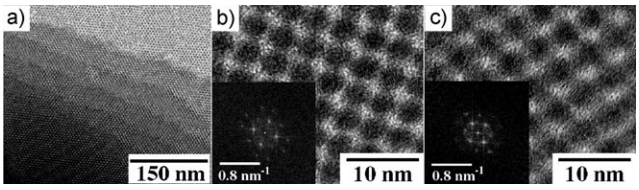

Figure 13. a) TEM image of three-dimensional arrangements of CdSe nanocrystals. b, c) HRTEM images of (100) and (110) projections along the CdSe superlattice with corresponding fast Fourier transformations.[1c]

of organometallic compounds such as dimethyl cadmium ($Cd(CH_3)_2$).[92] In the synthetic procedure involving organometallic precursors, most of the cadmium precursor is consumed by decomposition and the reaction with trioctylphosphineselenium (TOP-Se), which generates the nuclei immediately after injection of these reactants into the hot surfactant solution. The subsequent growth proceeds mainly through Ostwald ripening because of the low monomer concentration, and relatively polydisperse nanocrystals are produced. In contrast, the CdSe nuclei prepared from either cadmium oxide or cadmium acetate grow in the presence of a high monomer concentration in the size-focusing regime because the slow and gradual decomposition of the precursor results in a relatively high thermal stability of the precursors.[93] Mulvaney and co-workers reported a phosphine-free synthesis of CdSe nanocrystals. Se was dissolved in 1-octadecene at 200 °C to give a homogeneous Se stock solution that is stable at room temperature. This synthetic method does not require organometallic compounds of phophines and provides infomration on ligand effects on the growth dynamics and photophysics of CdSe nanocrystals.[94]

Similar synthetic routes were developed simultaneously by the Cao group. They showed that monodisperse CdSe nanocrystals were produced by slowly heating the reaction mixture to slightly above the decomposition temperature of cadmium myristate and the melting point of selenium. The relative standard deviation of the size of the CdSe nanocrystals produced by this method was below 5%.[95] This nonorganometallic route for synthesizing metal chalcogenide nanocrystals was extended to the preparation of various II–IV semiconductor nanocrystals, including PbSe, PbTe, ZnS, ZnSe, and CdS.[42a,96] Pradhan and Efrima synthesized uniform CdS nanocrystals by heating cadmium xanthate in a strong electron-donating solvent such as hexadecylamine at a relatively low temperature (70–120 °C).[97] The particle size was controlled by varying either the reaction temperature or the metal xanthate concentration. The Bawendi group fabricated a microstructured reactor for CdSe nanocrystals. This microfluidic system, composed of gas–liquid segmented flow, produces CdSe nanocrystals in a continuous and controllable manner with narrow size distributions and sizes that can be tuned by controlling cadmium and selenium precursor ratio.[98]

Peng and co-workers synthesized CdSe/CdS core/shell nanocrystals through successive ion layer adsorption and reaction (SILAR), whereby a CdS shell was grown one monolayer at a time by alternating the injections of the CdO precursor solution and sulfur solution into a reaction mixture containing the as-prepared CdSe core nanocrystals.[99] The photoluminescence quantum yield (PL QY) of the CdSe/CdS

core/shell nanocrystals ranged from 20 to 40%, and the PL full-width at half-maximum (fwhm) was between 23 and 26 nm. Under optimized reaction conditions, gram quantities of the core/shell nanocrystals were produced. Later, Mews and co-workers further extended the SILAR technique to synthesize CdSe-core $CdS/Zn_{0.5}Cd_{0.5}S/ZnS$ multishell nanocrystals. The nanocrystals exhibited a high fluorescence quantum yield (70–85%) for the amine-terminated multishell particles in organic solvents and a quantum yield of up to 50% for mercaptopropionic acid covered particles in water. These multishell nanocrystals possess superior photochemical and colloidal stability.[100] Ji, An, and co-workers synthesized nanocrystals of CdSe and CdSe/CdS core/shell with core sizes ranging from 1.2 to 1.5 nm and quantum yields of 60–80% from the two-phase thermolysis of Cd myristate and selenourea (thiourea) in the presence of oleic acid stabilizer in an autoclave.[101]

High temperature is required to form nuclei in the hot-injection method because the activation energy for nucleation is much higher than that for the growth of nanocrystals;[4a] this requirement is the major obstacle to large-scale production. Another approach for achieving monodisperse nanocrystals is to lower both the nucleation barrier and the growth temperature, which would minimize the Ostwald ripening process and produce uniform-sized nanocrystals. Several groups have used this procedure by inducing low-temperature reactions to form nuclei. Our group presented a generalized synthesis of various metal sulfide nanocrystals, which was based on a reaction between metal chlorides and elemental sulfur in the presence of oleylamine.[18d] In this method, sulfur in the oleylamine solution was added to the solution of the metal chloride–oleylamine complex at a relatively low temperature (ca. 140 °C), which caused a reaction between the metal ions and sulfur. Subsequent slow heating of the resulting reaction mixture produced metal sulfide nanocrystals with a narrow size distribution. Spherical CdS nanocrystals with sizes of 13 and 5.1 nm, and spherical 11-nm-sized ZnS nanocrystals were synthesized with this procedure. The synthetic procedure has many advantages over the conventional hot-injection route, such as the use of environmentally friendly and inexpensive reagents such as metal chlorides and sulfur, and large yields of uniform nanocrystals without the need for a size-selection procedure. Cao and Wang showed that the nucleation and growth stages could be effectively separated by nucleation initiators, such as tetraethylthiuram disulfide ($[(C_2H_5)_2NCS_2]_2$) and 2,2′-dithiobis(benzothiazole), in the synthesis of CdS nanocrystals.[102] As the standard deviation of these CdS nanocrystals from this method was 7%, defocusing did not occur.

Our group synthesized monodisperse 5-nm-sized quasi-spherical ZnS nanocrystals with a cubic zinc blende structure by adding diethylzinc ($Zn(C_2H_5)_2$) to sulfur dissolved in a mixture of hexadecylamine and 1-octadecene at 45 °C, and then aging at 300 °C.[103]

Basché and co-workers synthesized monodisperse type-II core/shell nanocrystals with a ZnTe core and a thin few-monolayer-thick shell of CdSe, CdS, and CdTe by a one-pot, high-temperature route by alternate addition of precursors (CdO, S, Se, or Te) into the crude reaction solution of monodisperse ZnTe cores.[104] The core/shell nanocrystals showed a narrow size distribution, and photoluminescence quantum yields of up to 30% have been obtained. The emission can be widely tuned from the visible to the near-IR region (550–900 nm) by increasing the thickness of the shell materials and by variation of the size ratio of core and shell.

5.2. Nanocrystals of PbS and PbSe

Colvin and co-workers synthesized monodisperse PbSe nanocrystals with diameters ranging from 3 to 13 nm from the reaction of PbO and TOP-Se in 1-octadecene in the presence of oleic acid.[96d] The Bawendi group synthesized uniform-sized PbSe nanocrystals from lead(II) acetate trihydrate ($Pb(Ac)_2{\cdot}3H_2O$) and TOP-Se in phenyl ether in the presence of oleic acid.[105] The reaction temperature, reaction time, and precursor concentration were used to vary the particle size from 2 to 10 nm. The Murray group synthesized PbSe nanocrytals from lead oleate and trioctylphosphine selenide. By varing the reaction temperature between 90 and 220 °C, the diamter of the nanocrystals could be controlled from 3.5 to 15 nm. The initial size distribution of 10% was further narrowed down to 5% by size-selective precipitation.[42a] Houtepen et al. reported that to obtain spherical PbSe nanocrystals it is crucial to use Pb–oleate precursors that are completely free of acetate. When acetate ions exist in the reaction mixture, star-shaped PbSe nanocrystals are formed by an oriented-attachment mechanism.[106]

Our group synthesized cube-shaped PbS nanocrystals with particle sizes of 6, 8, 9, and 13 nm from lead(II) chloride ($PbCl_2$) and elemental sulfur in oleylamine at 140 °C.[18d] The particle size was controlled by changing the relative amount of $PbCl_2$ and sulfur. Figure 14 shows a TEM image of the 13-nm PbS nanocrystals. Under optimized conditions, as much as 5 g of uniform cube-shaped PbS nanocrystals could be produced. Cademartiri, Ozin, and co-workers used monodisperse PbS nanocrystals for the fabrication of tailorable and patternable functional flexible films of densely packed nanocrystals exhibiting flexible near IR photoluminescence.[107]

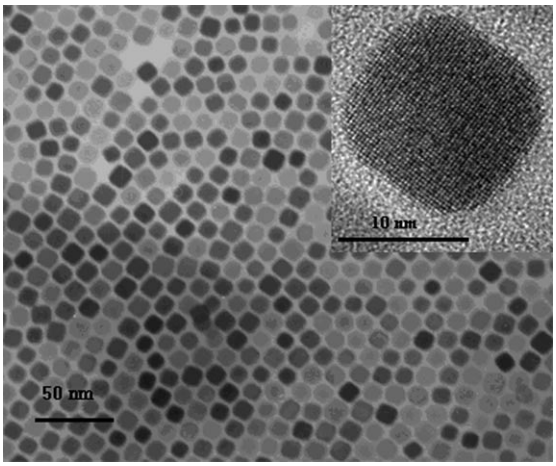

Figure 14. Low-magnification TEM image and HRTEM image (inset) of 13-nm PbS nanocrystals.[18d]

5.3. Copper Sulfide Nanocrystals

Korgel and co-workers demonstrated a solventless synthesis of monodisperse Cu_2S nanorods with a diameter of 4 nm and a length of 12 nm by thermolysis of a copper thiolate complex generated from copper octanoate and dodecanethiol.[108] Using a similar synthetic procedure, they synthesized Cu_2S nanodisks with shapes ranging from circular to hexagonal prisms, diameters ranging from 3 to 150 nm, and thicknesses ranging from 3 to 12 nm.[109] Chen and co-workers employed a reaction between copper acetylacetone and elemental sulfur in oleylamine at 230 °C to synthesize uniform-sized Cu_2S nanoplates with edge lengths of 9 nm and thicknesses of 4.5 nm.[110] The monodisperse hexagon nanoplates were self-assembled to form three-dimensional superlattices. Qian and co-workers synthesized monodisperse nanocrystals of PbS, Cu_2S, and Ag_2S through a reaction between the metal thiolate and thioacetamide in a pure dodecanethiol.[111] In the synthesis, the metal salts were dissolved in warm $C_{12}H_{25}SH$ to form metal thiolates, which were rapidly converted into metal sulfide nanocrystals after addition of thioacetamide (TAA). Monodisperse PbS nanocrystals with a diameter of 4.3 nm, Cu_2S nanocrystals that were slightly elongated with a length of 4.5 nm and a thickness of 3 nm, and 3.2-nm monodisperse Ag_2S nanocrystals were obtained by using this method. These monodisperse nanocrystals could self-assemble to form superlattice structures.

5.4. Cobalt Sulfide Nanocrystals

Alivisatos and co-workers synthesized hollow nanocrystals of cobalt sulfide and cobalt oxide through a mechanism analogous to the Kirkendall effect. Hollow cobalt sulfide nanospheres were synthesized by rapid injection of a sulfur solution into a cobalt nanocrystal dispersion at 475 K.[112] Two stable cobalt sulfide phases, linnaeite (Co_3S_4) and cobalt pentlandite (Co_9S_8), were observed depending on the molar ratio of sulfur and cobalt. Hollow cobalt oxide (CoO) nanocrystals were generated by oxidation of cobalt nanocrystals at 455 K for 3 h.

5.5. Nanocrystals of III–V Semiconductors

Nanocrystals of III–V semiconductors are known to be more difficult to synthesize than II–VI semiconductor nanocrystals because of the stronger covalent bonding of the precursors in III–V semiconductor nanocrystals, so that a high synthesis temperature and a long reaction time are required.[113] These conditions inevitably cause Ostwald ripening, which broadens the particle size distribution. In the following sections, the synthesis of III–V nanocrystals by dehalosilylation between metal halides and $P[Si(CH_3)_3]_3$ or $As[Si(CH_3)_3]_3$ at elevated temperature is discussed.

5.5.1. InP Nanocrystals

After the pioneering work by the Bawendi group on the synthesis of II–VI semiconductor nanocrystals, similar synthetic procedures have been used to synthesize nanocrystals of InP and GaP. The Nozik group synthesized InP nanocrystals with sizes ranging from 2 to 6.5 nm from the reaction of chloroindium oxalate and $P[Si(CH_3)_3]_3$ in a mixture of TOPO and TOP at 270 °C for 3 days.[114] The synthesized nanocrystals have a relatively uniform size distribution of about 10% standard deviation. However, the quantum yield was below 1% because of their significant sensitivity to surface trap states, which are caused by phosphorous surface vacancies and dangling bonds. These surface trap states could be eliminated by photochemical etching with HF or NH_4F under the illumination of light to give enhanced quantum yields up to 20–40%.[115] The Peng group synthesized high-quality InP nanocrystals with a narrow size distribution by using noncoordinating solvents such as octadecene and fatty acids as surface capping agents. The growth of InP nanocrystals takes place within a few hours when noncoordinating solvent was used, which is much faster than the previous results on the synthesis of III–V semiconductor nanocrystals using coordinating solvents.[116] Recently, Nann and co-workers synthesized monodisperse InP nanocrystals from $(CH_3)_3In$ and $P[Si(CH_3)_3]_3$ in weakly coordinating solvents such as methyl myristate or dibutyl sebacate.[117] In this approach, the reaction between highly reactive indium complex, produced from trimethylindium and methyl myristate or dibutyl sebacate, PH_3 generated in situ from $P[Si(CH_3)_3]_3$, and long-chain carboxylic acids (e.g. oleic acid) or long-chain alkyl amines (e.g. dioctylamines), accelerated the nucleation process.

5.5.2. InAs Nanocrystals

The Alivisatos group reported the synthesis of InAs nanocrystals from $InCl_3$ and $As[Si(CH_3)_3]_3$ at temperatures ranging from 240 and 265 °C in TOP.[118] Size-selective precipitation was employed to give relatively uniform nanocrystals with standard deviations of 10–15% because the as-synthesized nanocrystals were highly polydisperse. InAs nanocrystals with relatively narrow size distributions were produced by multiple injection of precursor into the reaction mixture through "focusing of size" during nanocrystals growth, which is similar to the synthesis of monodisperse CdSe nanocrystals.[7] Cao and Banin synthesized various core/shell semiconductor nanocrystals with InAs cores and III–V semiconductor shells (InP and GaAs) and II–VI semiconductor shells (CdSe, ZnSe, and ZnS) by using a two step synthesis.[119] In the first step, InAs cores were prepared, and in the second step the shells were grown by high-temperature pyrolysis of organometallic precursors in a coordinating solvent. When ZnSe or CdSe shells grow on InAs core nanocrystals, high-quality nanocrystals with quantum yields as high as 20% were produced.

6. Nanocrystals of Gold, Silver, and Platinum Group Metals

Colloidal nanoparticles of platinum group metals, particularly palladium and platinum, have attracted a great deal of attention owing to their many catalytic applications, including the hydrogenation of olefins, carbon–carbon coupling reactions, and electrocatalytic reactions for low-temperature fuel cells.[120] Recently, gold nanoparticles have been used in the field of biosensors, disease diagnosis, and gene expression.[121]

Large metal clusters of gold, platinum, and palladium ranging from 6–30 Å were synthesized by the reduction of metal ions with an appropriate reducing agent in the presence of phosphorous- and nitrogen-containing molecules such as triphenylphosphine and phenanthroline. There are many excellent review articles summarizing the synthesis of these metal nanoclusters;[121a,122] reports on the synthesis of monodisperse nanocrystals of gold, silver, and platinum group metals are summarized in Table 3.

6.1. Nanocrystals of Gold and Silver

Brust and co-workers reported a so-called two-phase (or biphasic) method for synthesizing relatively uniform-sized gold nanoparticles from the reduction of a gold salt in a toluene solution.[123a,b] In this process, hydrogen tetrachloroaurate ($HAuCl_4 \cdot 3H_2O$) dissolved in water was transferred into an alkanethiol solution in toluene by using tetraoctylammonium bromide (TOAB, $(octyl)_4N^+Br^-$) as a phase-transfer reagent. The subsequent reduction was performed by adding $NaBH_4$ to the solution with vigorous stirring. This biphasic method has been used extensively to synthesize gold nanoparticles as well as nanoparticles of other noble metals.[124] More recently, Cooper, Brust, and co-workers synthesized near-monodisperse gold nanoparticles with sizes of 1–4 nm by a single-step reduction of hydrogen tetrachloroaurate with sodium borohydride in the presence of a water-soluble alkyl thioether end-functionalized poly(methacrylic acid) stabilizer.[123c] The particle size was controlled precisely by the ratio of Au to capping ligand, and the particles are readily dispersible in both aqueous and nonaqueous solvents. Stucky and co-workers synthesized monodisperse gold nanoparticles by single-phase reduction of $AuPPh_3Cl$ with amine–borane complex in the presence of alkyl thiol.[123d] The synthesized nanoparticles were self-assembled to form colloidal crystals.

Miyake and co-workers were able to control the particle size of monodisperse gold nanoparticles by heat treatment in the solid state.[125] The initial dodecanethiol-stabilized 1.5-nm-sized gold nanoparticles, prepared by Brust's two-phase method, increased in size to 3.4, 5.4, and 6.8 nm by heating

Table 3: Synthesis of monodisperse nanocrystals of gold, silver, and platinum group metals.

Materials	Precursors/Reagents	Surfactants	Solvents	Method[a]	Ref.
Au	$HAuCl_4$, $NaAuCl_4/LiAlH_4$	$C_{12}SH$, $C_{12}E_5$	hexadecane	R	[16d]
	$AuCl_3$/TBAB, hydrazine	$C_{12}SH$, $C_{12}NH_2$, DA	toluene	R	[17c]
	$HAuCl_4$	linoleic acid, sodium linoleate	EtOH, H_2O	T	[31f]
	$HAuCl_4/NaBH_4$, TOAB	$C_{12}SH$	toluene, H_2O	R	[123a]
	$HAuCl_4/NaBH_4$, acetic acid	*p*-mercaptophenol	MeOH	R	[123b]
	$HAuCl_4/NaBH_4$	poly(methacrylic acid)	H_2O	R	[123c]
	$[AuCl(PPh_3)]$/amine–borane	$C_{12}SH$, $C_{12}NH_2$, PPh_3	benzene, $CHCl_3$	R	[123d]
	$HAuCl_4/NaBH_4$, TOAB	$C_{12}SH$, $C_{18}SH$	toluene, H_2O	R	[125]
	Au	$C_{12}SH$	acetone, toluene	E	[126a]
	$AuCl_3/NaBH_4$	$C_{12}SH$, $C_{12}NH_2$, $C_{18}SiH_3$, TOP	toluene	R[b]	[126b]
	$AuCl_3/NaBH_4$	$(C_8–C_{16})SH$	toluene	R[b]	[126c]
	$HAuCl_4$/EG, Ag NPs	PVP	EG	R	[130,132]
Pd	$[Pd(acac)_2]$/amine–borane	$C_{12}NH_2$	benzene	R	[123d]
	$PdCl_2$/alcohol	PVP	H_2O, MeOH, EtOH, 1-PrOH	R	[136]
	Na_2PdCl_4/EG	PVP	EG	R	[141]
	$[Pd(acac)_2]$	OAm, TOP	OAm, TOP	T	[144]
Ag	$Ag(Ac)_2$/TBAB, hydrazine	$C_{12}NH_2$, DA	toluene	R	[17c]
	$AgNO_3$	linoleic acid, sodium linoleate	EtOH, H_2O	T	[31f]
	$AgNO_3$/EG	PVP	EG	R	[40,130]
	$AgCF_3COO$/amine–borane	$C_{12}SH$	benzene	R	[123d]
	$AgCF_3COO$	OLEA	isoamyl ether	T, R	[135]
Pt	$PtCl_4$/TBAB	$C_{12}NH_2$	toluene	R	[17c]
	Pt salt	linoleic acid, sodium linoleate	EtOH, H_2O	T	[31f]
	H_2PtCl_6/EG, metal salt	PVP	EG	R	[138,139,142]
Ni/Pd	$NiSO_4$, $Pd(Ac)_2$/polyol	PVP	dioxane, glycol	R	[137]
	$[Ni(acac)_2]$, $[Pd(acac)_2]$	TOP	OAm	T	[146]
Rh	$RhCl_3$/EG	PVP	EG	R	[143]
Ru	$RuCl_3$/polyol	Na(Ac), $C_{12}SH$	propanediol, EG, bis(2-hydroxyethyl) ether	R	[148a]
	$[Ru(cod)(cot)]/H_2$	PVP, $(C_8–C_{16})NH_2$, $(C_8–C_{16})SH$	THF	R	[147b]
PtRu	$[Pt(dba)_2]$, $[Ru(cod)(cot)]/H_2$	PVP	THF	R	[149]
Ir	$[(MeC_5H_4)Ir(cod)]$/HDD	OLEA, OAm	OE	R	[150]

[a] T = thermal decomposition; R = reduction E = solvated metal atom dispersion (SMAD) with subsequent digestive ripening; [b] reduction with subsequent digestive ripening.

at 150, 190, and 230 °C, respectively. The authors suggested that particle growth was induced by the melting of the gold particle surface.

Jana and Peng reported a single-phase method for synthesizing uniform-sized gold nanoparticles.[17c] In this process, $AuCl_3$ dissolved in ammonium surfactants such as didodecyldimethylammonium bromide (DDAB, $(dodecyl)_2(CH_3)_2N^+Br^-$) was reduced with tetrabutylammonium borohydride (TBAB, $[CH_3(CH_2)_3]_4NBH_4$) with vigorous stirring. Fatty acids such as decanoic acid or aliphatic amines such as dodecylamine were added as ligands to control the particle size. Uniform-sized gold nanoparticles with particle sizes ranging from 1.5 to 7 nm could be synthesized by varying the experimental conditions. They also synthesized large (6–15 nm) gold nanocrystals by decreasing the reducing power of the reducing reagents by using a mixture of TBAB and hydrazine. They were able to synthesize uniform-sized nanoparticles of silver, copper, and platinum by a similar single-phase synthetic method.

Klabunde and co-workers reported a series of articles on the synthesis of monodisperse gold nanocrystals by a digestive-ripening process of polydisperse nanocrystals and the formation to superlattice structures of these monodisperse gold nanoparticles.[126,127] The initial polydisperse gold nanoparticles were produced either by reduction of gold chloride in reverse micelles or a solvated metal atom dispersion technique. In the reduction method, gold chloride was dissolved in toluene with an appropriate amount of didodecyldimethylammonium bromide and reduced with $NaBH_4$.[126b,c] Dodecanethiol was added to the resulting solution of polydisperse gold nanoparticles to ligate the gold surface through ligand exchange. The thiol-stabilized gold nanocrystals were then precipitated with ethanol, vacuum-dried, and redissolved into a solution of dodecanethiol in toluene. More dodecanethiol was added to the solution of thiol-stabilized gold nanoparticles, and the resulting mixture was heated at reflux for more than 10 min. The final nanoparticles were highly monodisperse with a diameter of 7 nm. The monodisperse gold nanocrystals were self-assembled into superlattice structures by drying a colloidal suspension on a solid surface. Dewetting could be controlled and gold nanocrystal superlattices with long-range ordering over several micrometers could be formed on silicon nitride substrates by adding nonvolatile dodecanethiol (Figure 15).[127c] Monolayer (two-dimensional) and bilayer (three-dimensional) superlattices could be produced by adjusting the nanocrystal concentration. Later, alkanethiols with different hydrocarbon chain lengths were found to function as good digestive ripening agents to produce highly monodisperse gold nanoparticles.[127a] However, the average particle size of the nanoparticles increased slightly from 4.5 to 5.5 nm as the digestive ripening ligands were changed from $C_8H_{17}SH$ to $C_{16}H_{33}SH$. More recently, other soft bases, including amines, silanes, and phosphines, were found to be efficient digestive-ripening ligands.[126a] The overall digestive-ripening process (Figure 16) was classified into three steps: 1) breaking of the polydisperse particles into smaller sized particles after adding the ligand (e.g. dodecanethiol), 2) removal of the side products to isolate the ligand-stabilized gold nanoparticles, and 3) heating of the isolated gold nanoparticles in the presence of the ligand to form monodisperse nanoparticles. Recently, the same group demonstrated the alloying reaction of copper (or silver) nanoparticles and gold nanoparticles by digestive ripening.[128] A mixture of gold nanoparticles and copper (or silver) nanoparticles in alkanethiol was refluxed to generate alloy nanoparticles of gold/silver or copper/gold. Interparticle diffusion of the atoms in nanoparticles is responsible for the formation of alloy nanoparticles.

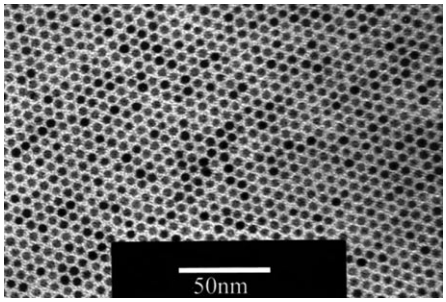

Figure 15. TEM image of two-dimensional self-assembled array of monodisperse 5.5-nm gold nanoparticles.[127c]

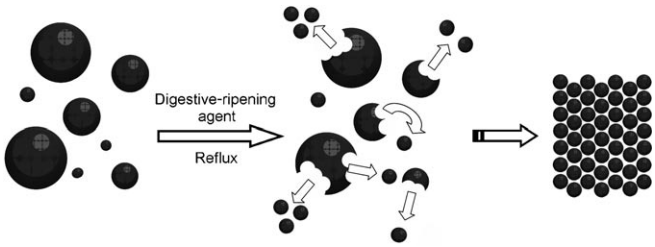

Figure 16. Schematic diagram showing the synthetic procedure for obtaining monodisperse nanoparticles by digestive ripening.

The Klabunde group also used a solvated metal atom dispersion technique (SMAD) to synthesize gram-scale quantities of gold nanoparticles. This technique involves the vaporization of a metal under vacuum and the co-deposition of gold atoms with the vapors of a solvent on the walls of a reactor cooled to 77 K. The as-synthesized polydisperse gold nanoparticles with diameters ranging from 5 to 40 nm were transformed into monodisperse gold nanoparticles with a diameter of 4.5 nm through a similar digestive-ripening process using dodecanethiol as a digestive-ripening ligand.[127b] These colloidal solutions of monodisperse gold nanoparticles have a tendency to self-assemble into two- and three-dimensional nanocrystal superlattice structures. The same group reported that monodisperse dodecanethiol-stabilized gold nanoparticles with similar average size self-assembled into different superlattice structures depending on the method used to prepare the nanocrystals.[127c] The nanoparticles synthesized by the reverse micelle technique preferentially assembled into face-centered cubic (fcc) structures, whereas gold nanoparticles obtained by the SMAD method organized into hexagonal close-packed (hcp) nanocrystal superlattices. The authors claimed that the different packing

behavior resulted from the differences in the degree of crystallinity of the nanoparticles synthesized by the two different synthetic methods. In other words, fcc ordering was preferred by single crystalline nanoparticles synthesized by the reverse micelle procedure, whereas hcp is the preferred structure of polycrystalline nanoparticles synthesized by the SMAD method.

Toshima and co-workers developed an alcohol-reduction method, which is a polyol process, for synthesizing noble-metal nanoparticles.[129] Noble-metal nanocrystals with various compositions, sizes, and shapes were synthesized in a polyol process by the reduction of metal salts with various alcohols as reducing agents in the presence of appropriate surfactants such as poly(vinylpyrrolidone) (PVP). More recently, the Xia group synthesized uniform-sized nanoparticles of silver, platinum, palladium, and gold by reduction of the metal salts with ethylene glycol (EG) in the presence of PVP.[40,130] The reduction of silver nitrate with ethylene glycol in the presence of PVP gave monodisperse silver nanocubes with a mean edge length of 175 nm. More recently, the same group was able to synthesize as much as 0.25 g of silver nanocubes with an average of size 130 nm by adding the appropriate amount of HCl to the polyol reaction mixture.[131] The authors suggested that HCl acted as selective etchant and material for dissolution of twinned silver nanoparticles. Through the use of silver nanocrystals as a sacrificial template for the galvanic replacement reaction in an aqueous solution, 30–200 nm silver nanocubes could be converted into gold nanoboxes.[132] Xia and co-workers investigated the mechanism of this transformation[132a,b] and suggested three major steps: 1) the reaction is initiated at a specific site with high surface energy; 2) nanoboxes with uniform and thin walls made of a silver-gold alloy are formed; 3) pores are formed in the walls as a result of the dealloying process. Changes in the molar ratio of silver and $HAuCl_4$ shifted the excitation peak of the gold nanostructures from the blue (400 nm) to the near-infrared (1200 nm) region.

The group of Yang synthesized various shaped gold nanocrystals with sizes ranging from 100 to 300 nm by using a modified polyol process.[133] $HAuCl_4{\cdot}3H_2O$ in ethylene glycol was boiled in the presence of PVP. Mainly triangular-shaped gold nanocrystals with sizes of approximately 210 nm were produced with a PVP and gold precursor molar ratio of 4.3, whereas gold nanocrystals with icosahedral shapes and sizes of about 230 nm were produced when the ratio was increased to 8.6. Uniform gold nanocubes with sizes of approximately 150 nm were produced when a small amount of silver ions were added to the reaction mixture. More recently, the Yang group synthesized polyhedral silver nanocrystals by periodic injection of silver nitrate and PVP into a hot pentanediol solution. By varying the duration of these sequential additions, silver nanocrystals of various polyhedral shapes were produced, including 80-nm-sized cubes, 120-nm-sized truncated cubes, 150–200-nm cuboctahedra, 200–250-nm truncated octahedra, and 250–300-nm octahedra.[134]

Wilcoxon and Provencio reported the synthesis of monodisperse gold nanocrystals by a seed-mediated growth approach.[16d] In the synthesis, gold and silver salts were reduced in the presence of 2-nm-sized gold nanocluster seeds. Monodisperse gold nanocrystals with particle sizes ranging from 2.6 to 5.7 nm could be produced by varying the amount of the gold precursors.

The Yang group demonstrated the synthesis of monodisperse silver nanoparticles with diameters ranging from 7 to 11 nm by thermal reduction of silver trifluoroacetate (CF_3CO_2Ag) in isoamyl ether with oleic acid. The particle sizes could be varied by changing the oleic acid to silver trifluoroacetate molar ratio.[135]

6.2. Nanocrystals of Platinum Group Metals

Polyol processes have been extensively used for synthesizing many Pt and Pd nanocrystals. Teranishi and Miyake synthesized monodisperse Pd nanoparticles by heating H_2PdCl_4 at reflux in a mixture of water and various alcohols in the presence of PVP.[136] The diameter of the nanoparticles could be controlled from 1.7 to 3.0 nm by changing the amount of PVP and the type and/or the concentration of alcohol in the solvent. Toshima and co-workers synthesized Ni/Pd bimetallic nanocrystals with a diameter of 1.9 nm by simultaneous polyol reduction of nickel(II) sulfate ($NiSO_4$) and palladium(II) acetate ($Pd(Ac)_2$) at 198 °C with ethylene glycol in the presence of PVP.[137]

The Xia group reported the morphological control of Pt nanoparticles by varying the amount of sodium nitrate ($NaNO_3$) added to the polyol reaction mixture, where hydrogen hexachloroplatinate(IV) (H_2PtCl_6) was reduced by ethylene glycol to form $PtCl_4^{2-}$ and Pt^0 at 160 °C.[138] The morphology of the Pt nanoparticles changed from irregular spheroids to tetrahedral and octahedral nanocrystals with well-defined facets as the molar ratio of $NaNO_3$ and H_2PtCl_6 was increased from 0 to 11. The Xia group also synthesized uniform 5-nm Pt nanocrystals by reduction of H_2PtCl_6 in ethylene glycol in the presence of PVP at 110 °C.[139] Pt nanostructures in the form of spheres, star-shaped particles, branched multipods, and uniform nanowires were generated when either $FeCl_3$ or $FeCl_2$ was added to the reaction mixture to manipulate the reduction kinetics of a polyol synthesis. The same group also synthesized cuboctahedral-shaped 8-nm-sized Pd nanoparticles by a modified polyol process, in which $[PdCl_4]^{2-}$ was reduced by ethylene glycol at 110 °C in the presence of PVP in air.[140] The key to the formation of uniform cuboctahedral nanoparticles was reported to be oxidative etching of twinned Pd nanoparticles by air. The Xia group demonstrated the role of oxygen or Fe^{III} species as oxidation etchants for the synthesis of Pd nanocubes or nanoboxes.[141] It was found that the concentration of $FeCl_3$ determined the number of seeds of Pd and the size of the Pd nanocubes.

The Yang group reported that a small amount of silver ions added to the polyol reaction mixture enhanced the crystal growth rate along ⟨100⟩, which essentially determines the shape and surface structure of the Pt nanocrystals. To prove this hypothesis, they synthesized monodisperse Pt nanocrystals with three different shapes: cubic, cuboctahedral, and octahedral particles with similar sizes (9–10 nm) were selectively produced by reduction of $H_2PtCl_6{\cdot}6H_2O$ in

boiling ethylene glycol in the presence of PVP and a small amount of silver nitrate ($AgNO_3$).[142]

Hoefelmeyer et al. synthesized cube-shaped rhodium nanocrystals with an edge length of 13 nm by reduction of rhodium(III) chloride ($RhCl_3$) in ethylene glycol in the presence of PVP at 190 °C.[143] In this process, 3.6-nm-sized seed particles were first generated by the reduction of $RhCl_3$ in ethylene glycol in the presence of PVP at 90 °C. These seed particles were subsequently used to produce larger 13-nm rhodium nanoparticles by reducing $RhCl_3$ at 190 °C in a homogeneous seeded-growth mechanism.

Our group synthesized monodisperse 3.5-nm-sized Pd nanoparticles by thermal decomposition of a Pd–TOP complex in TOP.[144] Pd nanoparticles with particle sizes of 5 and 7 nm were produced when a mixture of TOP and oleylamine was used as the surfactant and the solvent. Figure 17 shows

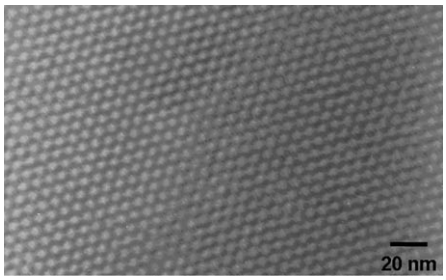

Figure 17. TEM image of three-dimensional superlattice structure of 3.5-nm-sized monodisperse Pd nanoparticles.[144]

the three-dimensional superlattice structure of the 3.5-nm-sized monodisperse Pd nanoparticles. Later, monodisperse palladium nanoparticles stabilized with various phosphine ligands could be synthesized by a surfactant-exchange reaction of the TOP-stabilized Pd nanoparticles by understanding their coordination chemistry.[145] These monodisperse nanoparticles include water-dispersible Pd nanoparticles and chiral-ligand-stabilized Pd nanoparticles.

Our group reported the synthesis of 4-nm-sized Pd–Ni bimetallic nanoparticles with a Ni-rich core/Pd-rich shell structure by thermal decomposition of Pd–TOP and Ni–TOP complexes.[146] The key to produce the Ni/Pd core/shell nanoparticles derived from the difference in the decomposition temperatures of the metal complexes: the Ni–TOP complex decomposes at around 205 °C, and the Pd–TOP complex above 230 °C. After aging the mixture at 205 °C for 30 min to decompose the Ni–TOP complex completely, the temperature was slowly increased to 235 °C to decompose the Pd–TOP complex, which generated the Pd shell on the top of the Ni core.

The Chaudret group reported the synthesis of polycrystalline ruthenium nanoparticles by an organometallic approach. The precursor [Ru(cod)(cot)] (cod = 1,5-cyclooctadiene, cot = 1,3,5-cyclooctatriene) was decomposed under an H_2 atmosphere in either pure alcohol or an alcohol/THF mixture.[147]

Viau and co-workers reported the synthesis of ruthenium nanoparticles by reduction of $RuCl_3$ in hydrophilic diols such as 1,2-propanediol or 1,2-ethanediol in the presence of acetate ions.[148] In this system, the diols were used as a solvent, a reductant, and a growth medium, and the acetate ion prevented the aggregation of ruthenium nanoparticles. The particle size could be controlled in the range 1.5–6 nm by varying the reaction temperature or the acetate concentration.

Chaudret and co-workers synthesized PtRu nanoparticles through the decomposition of [$Pt(dba)_2$] (dba = dibenzylidene acetone) and [Ru(cod)(cot)] under dihydrogen in the presence of PVP.[149] The Korgel group reported the synthesis of iridium nanocrystals by the reduction of methylcyclopentadienyl(1,5-cyclooctadiene)Ir with hexadecanediol in the presence of four different capping ligand combinations.[150]

7. Conclusions and Outlook

Over the last ten years, many different kinds of monodisperse spherical nanocrystals with controllable particle sizes and compositions have been synthesized by a wide range of chemical synthetic procedures: burst of nucleation followed by aging, the thermal decomposition of metal–surfactant complexes, nonhydrolytic sol–gel reactions, digestive-ripening processes, and polyol processes. For a generalized synthesis of monodisperse nanocrystals of various materials, more studies on the mechanisms of nucleation and growth during particle formation are needed. Because monodisperse nanocrystals of a wide variety of materials are now available, extensive studies on the size-dependent characteristics of these nanocrystals are expected. Some of the challenging materials in the synthesis of monodisperse nanocrystals include silicon, bi- and multimetallic oxides, doped materials, and core/shell materials. Although there are a few reports on the synthesis of these nanocrystals, monodisperse nanocrystals are rarely reported.

Intensive research has been conducted on the assembly of monodisperse nanocrystals to form two- and three- dimensional superlattice structures. These organized nanoparticles exhibit novel physical properties that derive from their collective interaction, and which are essential for their use in magnetic storage media and electronic devices.[151,29q,47,48,51b]

It is believed that the monodisperse nanocrystals will have many important applications in various areas including information technology, biotechnology, and energy/environmental technology. In particular, different kinds of nanocrystals have been extensively used in biomedical applications.[152] For example, magnetic nanocrystals have been applied to contrast enhancement agents for magnetic resonance imaging (MRI), magnetic carriers for drug-delivery systems (DDS), biosensors, and bioseparation.[153] Semiconductor nanocrystals have been applied as fluorescent probes for cell labeling, cell tracking, and cellular imaging.[90d,e,i,154] Gold nanoparticles derivatized with oigonucleotides were capable of sensing complementary DNA strands detectable by color changes resulting from the shift of surface plasmon resonance peaks from isolated to aggregated nanoparticles.[155] Most of the monodisperse nanocrystals have been synthesized in organic media, and their transfer to the

aqueous phase and their functionalization are very important for their extensive biomedical applications.[156] Immobilization of monodisperse nanocrystals into appropriate matrices will be important for many biomedical applications, including targeted drug delivery and multimodal imaging.[157] Finally, large-scale synthetic procedures should be further developed to realize the extensive applications of these monodisperse nanocrystals.[18a]

Abbreviations

1-PrOH	1-propanol
Ac	acetate
ACA	1-adamantanecarboxilic acid
acac	acetylacetonate
AOT	bis(2-ethylhexyl)sulfosuccinate
BA	1-benzoylacetonate
$C_{12}SH$	dodecanethiol
$C_{16}SH$	hexadecanethiol
$C_{18}SH$	octadecanethiol
C_8SH	octanethiol
cod	1,5-cyclooctadiene
cot	1,3,5-cyclooctatriene
Cp	cyclopentanedienyl
Cup	cupferron
DA	decanoic acid
dba	dibenzylidene acetone
DDA, $C_{12}NH_2$	dodecylamine
EG	ethylene glycol
HDA, $C_{16}NH_2$	hexadecylamine
HDAC	hexadecylamonium chloride
HDD	hexacanediol
LA	lauric acid
OAm	oleylamine
ODA, $C_{18}NH_2$	octadecylamine
ODE	1-octadecene
OE	octyl ether
OLEA	oleic acid
PE	phenyl ether
PVP	poly(vinyl pyrrolidone)
SA	stearic acid
TBAB	tetrabutylammonium borohydride
TBP	tributylphosphine
TDPA	tetradecylphosphonic acid
TMNO	trimethylamine *N*-oxide
TMPPA	bis(2,2,4-trimethylphenyl)phosphinic acid
TOA	trioctylamine
TOP	trioctylphosphine
TOPO	trioctylphosphine oxide

We thank the Korean Ministry of Science and Technology for the funding through the National Creative Research Initiative Program of the Korea Science and Engineering Foundation (KOSEF).

Received: August 3, 2006
Published online: May 24, 2007

[1] a) G. Schmid, *Nanoparticles: From Theory to Application*, Wiley-VCH, Weinheim, **2004**; b) K. J. Klabunde, *Nanoscale Materials in Chemistry*, Wiley-Interscience, New York, **2001**; c) A. L. Rogach, D. V. Talapin, E. V. Shevchenko, A. Kornowski, M. Haase, H. Weller, *Adv. Funct. Mater.* **2002**, *12*, 653; d) J. H. Fendler, *Nanoparticles and Nanostructured Films*, Wiley-VCH, Weinheim, **1998**; e) T. Hyeon, *Chem. Commun.* **2003**, 927.

[2] a) S. Sun, C. B. Murray, D. Weller, L. Folks, A. Moser, *Science* **2000**, *287*, 1989; b) D. E. Speliotis, *J. Magn. Magn. Mater.* **1999**, *193*, 29; c) R. C. O'Handley, *Modern Magnetic Materials: Principles and Applications*, Wiley-Interscience, New York, **1999**.

[3] a) Y. Xia, P. Yang, Y. Sun, Y. Wu, B. Mayers, B. Gates, Y. Yin, F. Kim, H. Yan, *Adv. Mater.* **2003**, *15*, 353; b) A special issue on nanowires: *Adv. Mater.* **2003**, *15*, 351; c) H. J. Fan, P. Werner, M. Zacharias, *Small* **2006**, *2*, 700; d) Y.-w. Jun, J.-s. Choi, J. Cheon, *Angew. Chem.* **2006**, *118*, 3092; *Angew. Chem. Int. Ed.* **2006**, *45*, 3414; e) C. Burda, X. Chen, R. Narayanan, M. A. El-Sayed, *Chem. Rev.* **2005**, *105*, 1025; f) S. Kumar, T. Nann, *Small* **2006**, *2*, 316; g) Y. Yin, A. P. Alivisatos, *Nature* **2005**, *437*, 664; h) S. Eustis, M, A. El-Sayed, *Chem. Soc. Rev.* **2006**, *35*, 209.

[4] a) T. Sugimoto, *Monodispersed Particles*, Elsevier, Amsterdam, **2001**; b) T. Sugimoto, *Adv. Colloid Interface Sci.* **1987**, *28*, 65.

[5] V. K. LaMer, R. H. Dinegar, *J. Am. Chem. Soc.* **1950**, *72*, 4847.

[6] Z. A. Peng, X. Peng, *J. Am. Chem. Soc.* **2002**, *124*, 3343.

[7] X. Peng, J. Wickham, A. P. Alivisatos, *J. Am. Chem. Soc.* **1998**, *120*, 5343.

[8] J. W. Mullin, *Crystallization*, 3rd ed., Oxford University Press, Oxford, **1997**.

[9] a) T. Vossmeyer, L. Katsikas, M. Giersig, I. G. Popovic, K. Diesner, A. Chemseddine, A. Eychmüller, H. Weller, *J. Phys. Chem.* **1994**, *98*, 7665; b) L. Spanhel, M. A. Anderson, *J. Am. Chem. Soc.* **1991**, *113*, 2826.

[10] A. P. Alivisatos, *J. Phys. Chem.* **1996**, *100*, 13226.

[11] a) R. C. Garvie, *J. Phys. Chem.* **1978**, *82*, 218; b) H. Zhang, J. F. Banfield, *J. Phys. Chem. B* **2000**, *104*, 3481.

[12] a) C. B. Murray, D. J. Norris, M. G. Bawendi, *J. Am. Chem. Soc.* **1993**, *115*, 8706; b) C. B. Murray, C. R. Kagan, M. G. Bawendi, *Annu. Rev. Mater. Sci.* **2000**, *30*, 545.

[13] a) G. Schmid, N. Klein, B. Morun, A. Lehnert, *Pure Appl. Chem.* **1990**, *62*, 1175; b) M. M. Alvarez, J. T. Khoury, T. G. Schaaff, M. Shafigullin, I. Vezmar, R. L. Whetten, *Chem. Phys. Lett.* **1997**, *266*, 91; c) M. N. Vargaftik, V. P. Zagorodnikov, I. P. Stolarov, I. I. Moiseev, D. I. Kochubey, V. A. Likholobov, A. L. Chuvilin, K. I. Zamaraev, *J. Mol. Catal.* **1989**, *53*, 315; d) J. D. Aiken III, Y. Lin, R. G. Finke, *J. Mol. Catal. A* **1996**, *114*, 29; e) M. A. Watzky, R. G. Finke, *J. Am. Chem. Soc.* **1997**, *119*, 10382; f) I. L. Garzón, K. Michaelian, M. R. Beltrán, A. Posada-Amarillas, P. Ordejón, E. Artacho, D. Sánchez-Portal, J. M. Soler, *Phys. Rev. Lett.* **1998**, *81*, 1600.

[14] a) T. Vossmeyer, G. Reck, L. Katsikas, E. T. K. Haupt, B. Schulz, H. Weller, *Science* **1995**, *267*, 1476; b) S. Behrens, M. Bettenhausen, A. C. Deveson, A. Eichhöfer, D. Fenske, A. Lohde, U. Woggon, *Angew. Chem.* **1996**, *108*, 2360; *Angew. Chem. Int. Ed. Engl.* **1996**, *35*, 2215; c) V. N. Soloviev, A. Eichhöfer, D. Fenske, U. Banin, *J. Am. Chem. Soc.* **2001**, *123*, 2354.

[15] R. Jose, N. U. Zhanpeisov, H. Fukumura, Y. Baba, M. Ishikawa, *J. Am. Chem. Soc.* **2006**, *128*, 629.

[16] a) N. R. Jana, L. Gearheart, C. J. Murphy, *Chem. Mater.* **2001**, *13*, 2313; b) H. Yu, P. C. Gibbons, K. F. Kelton, W. E. Buhro, *J. Am. Chem. Soc.* **2001**, *123*, 9198; c) J. Park, E. Lee, N. M. Hwang, M. Kang, S. C. Kim, Y. Hwang, J. G. Park, H. J. Noh, J. Y. Kim, J. H. Park, T. Hyeon, *Angew. Chem.* **2005**, *117*, 2932;

Angew. Chem. Int. Ed. **2005**, *44*, 2872; d) J. P. Wilcoxon, P. P. Provencio, *J. Am. Chem. Soc.* **2004**, *126*, 6402.

[17] a) D. V. Talapin, A. L. Rogach, A. Kornowski, M. Haase, H. Weller, *Nano Lett.* **2001**, *1*, 207; b) J. Hambrock, R. Becker, A. Birkner, J. Weiß, R. A. Fischer, *Chem. Commun.* **2002**, 68; c) N. R. Jana, X. Peng, *J. Am. Chem. Soc.* **2003**, *125*, 14280.

[18] a) J. Park, K. An, Y. Hwang, J. G. Park, H. J. Noh, J. Y. Kim, J. H. Park, N. M. Hwang, T. Hyeon, *Nat. Mater.* **2004**, *3*, 891; b) W. S. Seo, H. H. Jo, K. Lee, J. T. Park, *Adv. Mater.* **2003**, *15*, 795; c) W. W. Yu, J. C. Falkner, C. T. Yavuz, V. L. Colvin, *Chem. Commun.* **2004**, 2306; d) J. Joo, H. B. Na, T. Yu, J. H. Yu, Y. W. Kim, F. Wu, J. Z. Zhang, T. Hyeon, *J. Am. Chem. Soc.* **2003**, *125*, 11100.

[19] a) C. R. Bullen, P. Mulvaney, *Nano Lett.* **2004**, *4*, 2303; b) M. Tiemann, Ö. Weiß, J. Hartikainen, F. Marlow, M. Lindén, *ChemPhysChem* **2005**, *6*, 2113; c) S. Asokan, K. M. Krueger, A. Alkhawaldeh, A. R. Carreon, Z. Mu, V. L. Colvin, N. V. Mantzaris, M. S. Wong, *Nanotechnology* **2005**, *16*, 2000; d) J. van Embden, P. Mulvaney, *Langmuir* **2005**, *21*, 10226.

[20] a) M. G. Bawendi, M. L. Steigerwald, L. E. Brus, *Annu. Rev. Phys. Chem.* **1990**, *41*, 477; b) A. P. Alivisatos, *Science* **1996**, *271*, 933.

[21] a) W. W. Yu, L. Qu, W. Guo, X. Peng, *Chem. Mater.* **2003**, *15*, 2854; b) O. Schmelz, A. Mews, T. Basché, A. Herrmann, K. Müllen, *Langmuir* **2001**, *17*, 2861.

[22] C. de Mello Donega, P. Liljeroth, D. Vanmaekelbergh, *Small* **2005**, *1*, 1152.

[23] Y. De Smet, L. Deriemaeker, R. Finsy, *Langmuir* **1997**, *13*, 6884.

[24] The nucleation rate was calculated from Equation (4) and the growth rate from Equation (23). $\alpha = 0.5$, $V_m = 3.29 \times 10^{-5}\,m^3\,mol^{-1}$, $C^{\circ}_{S,eq} = 1\,mol\,m^{-3}$, $K = 0.1$, $r_0 = 0.5\,nm$ and the volume of the reaction solution was $1.66 \times 10^{-19}\,m^{-3}$. The parameters S, T, γ, A, D, and Δt were varied for different simulations as stated in the text. The software used to run the simulation program was MATLAB 6.5.

[25] H. Reiss, *J. Chem. Phys.* **1951**, *19*, 482.

[26] a) D. V. Talapin, A. L. Rogach, M. Haase, H. Weller, *J. Phys. Chem. B* **2001**, *105*, 12278; b) D. V. Talapin, A. L. Rogach, E. V. Shevchenko, A. Kornowski, M. Haase, H. Weller, *J. Am. Chem. Soc.* **2002**, *124*, 5782.

[27] a) T. J. Trentler, T. E. Denler, J. F. Bertone, A. Agrawal, V. L. Colvin, *J. Am. Chem. Soc.* **1999**, *121*, 1613; b) J. Joo, T. Yu, Y. W. Kim, H. M. Park, F. Wu, J. Z. Zhang, T. Hyeon, *J. Am. Chem. Soc.* **2003**, *125*, 6553; c) S. Sun, C. B. Murray, *J. Appl. Phys.* **1999**, *85*, 4325.

[28] a) G. Herzer, *IEEE Trans.* **1989**, *MAG-25*, 3327; b) I. Skorvanek, R. C. O'Handley, *J. Magn. Magn. Mater.* **1995**, *140*, 467.

[29] a) N. Moumen, M. P. Pileni, *Chem. Mater.* **1996**, *8*, 1128; b) A. T. Ngo, M. P. Pileni, *Adv. Mater.* **2000**, *12*, 276; c) C. Petit, A. Taleb, M. P. Pileni, *Adv. Mater.* **1998**, *10*, 259; d) C. Liu, B. Zou, A. J. Rondinone, Z. J. Zhang, *J. Am. Chem. Soc.* **2000**, *122*, 6263; e) A. J. Rondinone, A. C. S. Samia, Z. J. Zhang, *J. Phys. Chem. B* **2000**, *104*, 7919; f) A. J. Rondinone, A. C. S. Samia, Z. J. Zhang, *J. Phys. Chem. B* **1999**, *103*, 6876; g) C. Liu, B. Zou, A. J. Rondinone, Z. J. Zhang, *J. Phys. Chem. B* **2000**, *104*, 1141; h) Y. S. Kang, S. Risbud, J. F. Rabolt, P. Stroeve, *Chem. Mater.* **1996**, *8*, 2209; i) J. P. Chen, C. M. Sorensen, K. J. Klabunde, G. C. Hadjipanayis, E. Devlin, A. Kostikas, *Phys. Rev. B* **1996**, *54*, 9288; j) Z. J. Zhang, Z. L. Wang, B. C. Chakoumakos, J. S. Yin, *J. Am. Chem. Soc.* **1998**, *120*, 1800; k) C. Y. Hong, I. J. Jang, H. E. Horng, C. J. Hsu, Y. D. Yao, H. C. Yang, *J. Appl. Phys.* **1997**, *81*, 4275; l) E. E. Carpenter, C. J. O'Connor, *J. Appl. Phys.* **1999**, *85*, 5175; m) C. R. Vestal, Z. J. Zhang, *J. Am. Chem. Soc.* **2003**, *125*, 9828; n) Y. Lalatonne, J. Richardi, M. P. Pileni, *Nat. Mater.* **2004**, *3*, 121; o) N. Feltin, M. P. Pileni, *Langmuir* **1997**, *13*, 3927; p) A. T. Ngo, M. P. Pileni, *J. Phys. Chem. B* **2001**, *105*, 53; q) I. Lisiecki, P. A. Albouy, M. P. Pileni, *Adv. Mater.* **2003**, *15*, 712; r) N. Mounmen, M. P. Pileni, *J. Phys. Chem.* **1996**, *100*, 1867.

[30] a) Z. X. Tang, C. M. Sorensen, K. J. Klabunde, G. C. Hadjipanayis, *J. Colloid Interface Sci.* **1991**, *146*, 38; b) J. P. Chen, K. M. Lee, C. M. Sorensen, K. J. Klabunde, G. C. Hadjipanayis, *J. Appl. Phys.* **1994**, *75*, 5876; c) S. Sun, C. B. Murray, H. Doyle, *Mater. Res. Soc. Symp. Proc.* **1999**, *577*, 385.

[31] a) S. J. Park, S. Kim, S. Lee, Z. G. Khim, K. Char, T. Hyeon, *J. Am. Chem. Soc.* **2000**, *122*, 8581; b) N. Cordente, M. Respaud, F. Senocq, M. J. Casanove, C. Amiens, B. Chaudret, *Nano Lett.* **2001**, *1*, 565; c) F. Dumestre, B. Chaudret, C. Amiens, M. Respaud, P. Fejes, P. Renaud, P. Zurcher, *Angew. Chem.* **2003**, *115*, 5371; *Angew. Chem. Int. Ed.* **2003**, *42*, 5213; d) F. Dumestre, B. Chaudret, C. Amiens, M.-C Fromen, M.-J Casanove, P. Renaud, P. Zurcher, *Angew. Chem.* **2002**, *114*, 4462; *Angew. Chem. Int. Ed.* **2002**, *41*, 4286; e) V. F. Puntes, K. M. Krishan, A. P. Alivisatos, *Science* **2001**, *291*, 2115; f) X. Wang, J. Zhuang, Q. Peng, Y. Li, *Nature* **2005**, *437*, 121.

[32] a) T. Hyeon, S. S. Lee, J. Park, Y. Chung, H. B. Na, *J. Am. Chem. Soc.* **2001**, *123*, 12798; b) J. Park, E. Kang, C. J. Bae, J. G. Park, H. J. Noh, J. Y. Kim, J. H. Park, H. M. Park, T. Hyeon, *J. Phys. Chem. B* **2004**, *108*, 13598.

[33] M. Faraday, *Philos. Trans. R. Soc. London* **1857**, *147*, 145.

[34] B. V. Enustun, J. Turkevich, *J. Am. Chem. Soc.* **1963**, *85*, 3317.

[35] M. P. Pileni, B. W. Ninham, T. Gulik-Krzywicki, J. Tanori, I. Lisiecki, A. Filankembo, *Adv. Mater.* **1999**, *11*, 1358.

[36] M. Maillard, S. Giorgio, M. P. Pileni, *Adv. Mater.* **2002**, *14*, 1084.

[37] a) M. P. Pileni, *Langmuir* **1997**, *13*, 3266; b) M. P. Pileni, *Nat. Mater.* **2003**, *2*, 145.

[38] D. Ingert, M. P. Pileni, *Adv. Funct. Mater.* **2001**, *11*, 136.

[39] H. Bönnemann, W. Brijoux, R. Brinkmann, E. Dinjus, T. Jaussen, B. Korall, *Angew. Chem.* **1991**, *103*, 1344; *Angew. Chem. Int. Ed. Engl.* **1991**, *30*, 1312.

[40] B. Wiley, Y. Sun, B. Mayers, Y. Xia, *Chem. Eur. J.* **2005**, *11*, 454.

[41] a) C. J. Brinker, G. W. Scherer, *Sol–Gel Science: The Physics and Chemistry of Sol–Gel Processing*, Academic Press, Boston, **1990**; b) A. Vioux, *Chem. Mater.* **1997**, *9*, 2292.

[42] a) C. B. Murray, S. Sun, W. Gaschler, H. Doyle, T. A. Betley, C. R. Kagan, *IBM J. Res. Dev.* **2001**, *45*, 47; b) C. B. Murray, S. Sun, H. Doyle, T. A. Betley, *MRS Bull.* **2001**, *26*, 985.

[43] V. F. Puntes, K. M. Krishnan, A. P. Alivisatos, *Appl. Phys. Lett.* **2001**, *78*, 2187.

[44] C. Petit, A. Taleb, M. P. Pileni, *J. Phys. Chem. B* **1999**, *103*, 1805.

[45] C. Petit, T. Cren, D. Roditchev, W. Sacks, J. Klein, M. P. Pileni, *Adv. Mater.* **1999**, *11*, 1198.

[46] a) D. Farrell, S. A. Majetich, J. P. Wilcoxon, *J. Phys. Chem. B* **2003**, *107*, 11022; b) S. Peng, C. Wang, J. Xie, S. Sun, *J. Am. Chem. Soc.* **2006**, *128*, 10676.

[47] F. Dumestre, B. Chaudret, C. Amiens, P. Renaud, P. Fejes, *Science* **2004**, *303*, 821.

[48] a) E. Shevchenko, D. Talapin, A. Kornowski, F. Wiehorst, J. Koetzler, M. Haase, A. Rogach, H. Weller, *Adv. Mater.* **2002**, *14*, 287; b) L. C. Varanda, M. Jafelicci, Jr., *J. Am. Chem. Soc.* **2006**, *128*, 11062; c) S. Sun, *Adv. Mater.* **2006**, *18*, 393.

[49] M. Chen, J. P. Liu, S. Sun, *J. Am. Chem. Soc.* **2004**, *126*, 8394.

[50] C. Liu, X. Wu, T. Klemmer, N. Shukla, X. Yang, D. Weller, A. G. Roy, M. Tanase, D. Laughlin, *J. Phys. Chem. B* **2004**, *108*, 6121.

[51] a) E. V. Shevchenko, D. V. Talapin, A. L. Rogach, A. Kornowski, M. Haase, H. Weller, *J. Am. Chem. Soc.* **2002**, *124*, 11480; b) E. V. Shevchenko, D. V. Talapin, H. Schnablegger, A. Kornowski, Ö. Festin, P. Svedlindh, M. Haase, H. Weller, *J. Am. Chem. Soc.* **2003**, *125*, 9090.

[52] M. Chen, D. E. Nikles, *J. Appl. Phys.* **2002**, *91*, 8477.

[53] M. Chen, D. E. Nikles, *Nano Lett.* **2002**, *2*, 211.

[54] a) J. I. Park, J. Cheon, *J. Am. Chem. Soc.* **2001**, *123*, 5743; b) W.-r. Lee, M. G. Kim, J.-r. Choi, J.-I. Park, S. J. Ko, S. J. Oh, J. Cheon, *J. Am. Chem. Soc.* **2005**, *127*, 16090.
[55] J. Rockenberger, E. C. Scher, A. P. Alivisatos, *J. Am. Chem. Soc.* **1999**, *121*, 11595.
[56] Y. Matsui, K. Nishio, H. Masuda, *Small* **2006**, *2*, 522.
[57] K. Woo, J. Hong, S. Choi, H. W. Lee, J. P. Ahn, C. S. Kim, S. W. Lee, *Chem. Mater.* **2004**, *16*, 2814.
[58] T. Hyeon, Y. Chung, J. Park, S. S. Lee, Y. W. Kim, B. H. Park, *J. Phys. Chem. B* **2002**, *106*, 6831.
[59] E. Kang, J. Park, Y. Hwang, M. Kang, J. G. Park, T. Hyeon, *J. Phys. Chem. B* **2004**, *108*, 13932.
[60] T. Fried, G. Shemer, G. Markovich, *Adv. Mater.* **2001**, *13*, 1158.
[61] S. Sun, H. Zeng, *J. Am. Chem. Soc.* **2002**, *124*, 8204.
[62] S. Sun, H. Zeng, D. B. Robinson, S. Raoux, P. M. Rice, S. X. Wang, G. Li, *J. Am. Chem. Soc.* **2004**, *126*, 273.
[63] H. Zeng, P. M. Rice, S. X. Wang, S. Sun, *J. Am. Chem. Soc.* **2004**, *126*, 11458.
[64] Q. Song, Z. J. Zhang, *J. Am. Chem. Soc.* **2004**, *126*, 6164.
[65] N. R. Jana, Y. Chen, X. Peng, *Chem. Mater.* **2004**, *16*, 3931.
[66] a) B. O'Regan, M. Grätzel, *Nature* **1991**, *353*, 737; b) A. Hagfeldt, M. Grätzel, *Chem. Rev.* **1995**, *95*, 49; c) S. G. Yan, J. S. Prieskorn, Y. J. Kim, J. T. Hupp, *J. Phys. Chem. B* **2000**, *104*, 10871; d) P. V. Kamat, *Chem. Rev.* **1993**, *93*, 267; e) Y. Cho, W. Choi, C. H. Lee, T. Hyeon, H. I. Lee, *Environ. Sci. Technol.* **2001**, *35*, 2988; f) K. Iuchi, Y. Ohko, T. Tatsuma, A. Fujishima, *Chem. Mater.* **2004**, *16*, 1165.
[67] a) J. Lin, Y. Lin, P. Liu, M. J. Meziani, L. F. Allard, Y. Sun, *J. Am. Chem. Soc.* **2002**, *124*, 11514; b) C. Feldmann, H. O. Jungk, *Angew. Chem.* **2001**, *113*, 372; *Angew. Chem. Int. Ed.* **2001**, *40*, 359; c) T. Kasuga, M. Hiramatsu, A. Hoson, T. Sekino, K. Niihara, *Adv. Mater.* **1999**, *11*, 1307; d) Q. Chen, W. Zhou, G. Du, L. Peng, *Adv. Mater.* **2002**, *14*, 1208.
[68] a) T. Moritz, J. Reiss, K. Diesner, D. Su, A. Chemseddine, *J. Phys. Chem. B* **1997**, *101*, 8052; b) A. Chemseddine, T. Moritz, *Eur. J. Inorg. Chem.* **1999**, 235.
[69] S. O'Brien, L. Brus, C. B. Murray, *J. Am. Chem. Soc.* **2001**, *123*, 12085.
[70] J. Tang, J. Fabbri, R. D. Robinson, Y. Zhu, I. P. Herman, M. L. Steigerwald, L. E. Brus, *Chem. Mater.* **2004**, *16*, 1336.
[71] J. Joo, S. G. Kwon, J. H. Yu, T. Hyeon, *Adv. Mater.* **2005**, *17*, 1873.
[72] M. L. Kahn, M. Monge, E. Snoeck, A. Maisonnat, B. Chaudret, *Small* **2005**, *1*, 221.
[73] L. Gou, C. J. Murphy, *Nano Lett.* **2003**, *3*, 231.
[74] S. U. Son, I. K. Park, J. Park, T. Hyeon, *Chem. Commun.* **2004**, 778.
[75] M. Yin, C. K. Wu, Y. Lou, C. Burda, J. T. Koberstein, Y. Zhu, S. O'Brien, *J. Am. Chem. Soc.* **2005**, *127*, 9506.
[76] M. Yin, S. O'Brien, *J. Am. Chem. Soc.* **2003**, *125*, 10180.
[77] W. S. Seo, H. H. Jo, K. Lee, B. Kim, S. J. Oh, J. T. Park, *Angew. Chem.* **2004**, *116*, 1135; *Angew. Chem. Int. Ed.* **2004**, *43*, 1115.
[78] X. Sun, Y. W. Zhang, R. Si, C. H. Yan, *Small* **2005**, *1*, 1081.
[79] F. X. Redl, C. T. Black, G. C. Papaefthymiou, R. L. Sandstrom, M. Yin, H. Zeng, C. B. Murray, S. P. O'Brien, *J. Am. Chem. Soc.* **2004**, *126*, 14583.
[80] T. He, D. Chen, X. Jiao, *Chem. Mater.* **2004**, *16*, 737.
[81] a) J. Park, E. Kang, S. U. Son, H. M. Park, M. K. Kim, J. Kim, K. W. Kim, H. J. Noh, J. H. Park, C. Bae, J. G. Park, T. Hyeon, *Adv. Mater.* **2005**, *17*, 429; b) I. S. Lee, N. Lee, J. Park, B.-H. Kim, Y.-W. Yi, T. Kim, T. K. Kim, I. H. Lee, S. R. Paik, T. Hyeon, *J. Am. Chem. Soc.* **2006**, *128*, 10658.
[82] S. U. Son, Y. Jang, K. Y. Yoon, C. An, Y. Hwang, J. G. Park, H. J. Noh, J. Y. Kim, J. H. Park, T. Hyeon, *Chem. Commun.* **2005**, 86.
[83] K. Soulantica, A. Maisonnat, M. C. Fromen, M. J. Casanove, B. Chaudret, *Angew. Chem.* **2003**, *115*, 1989; *Angew. Chem. Int. Ed.* **2003**, *42*, 1945.
[84] K. Soulantica, A. Maisonnat, M. C. Fromen, M. J. Casanove, P. Lecante, B. Chaudret, *Angew. Chem.* **2001**, *113*, 462; *Angew. Chem. Int. Ed.* **2001**, *40*, 448.
[85] Q. Liu, W. Lu, A. Ma, J. Tang, J. Lin, J. Fang, *J. Am. Chem. Soc.* **2005**, *127*, 5276.
[86] Y. C. Cao, *J. Am. Chem. Soc.* **2004**, *126*, 7456.
[87] R. Si, Y. W. Zhang, L. P. You, C. H. Yan, *Angew. Chem.* **2005**, *117*, 3320; *Angew. Chem. Int. Ed.* **2005**, *44*, 3256.
[88] T. Yu, J. Joo, Y. I. Park, T. Hyeon, *Angew. Chem.* **2005**, *117*, 7577; *Angew. Chem. Int. Ed.* **2005**, *44*, 7411.
[89] E. H. Sargent, *Adv. Mater.* **2005**, *17*, 515.
[90] a) J. Hu, L. S. Li, W. Yang, L. Manna, L. W. Wang, A. P. Alivisatos, *Science* **2001**, *292*, 2060; b) V. C. Sundar, H. J. Eisler, M. G. Bawendi, *Adv. Mater.* **2002**, *14*, 739; c) N. Tessler, V. Medvedev, M. Kazes, S. Kan, U. Banin, *Science* **2002**, *295*, 1506; d) M. P. Brunchez, M. Moronne, P. Gin, S. Weiss, A. P. Alivisatos, *Science* **1998**, *281*, 2013; e) W. C. Chan, S. Nie, *Science* **1998**, *281*, 2016; f) M. Achermann, M. A. Petruska, S. Kos, D. L. Smith, D. D. Koleske, V. I. Klimov, *Nature* **2004**, *429*, 642; g) W. U. Huynh, J. J. Dittmer, A. P. Alivisatos, *Science* **2002**, *295*, 2425; h) R. D. Schaller, V. I. Klimov, *Phys. Rev. Lett.* **2004**, *92*, 186601; i) A. P. Alivisatos, *Nat. Biotechnol.* **2004**, *22*, 47; j) S. Kim, Y. T. Lim, E. G. Soltesz, A. M. De Grand, J. Lee, A. Nakayama, J. A. Parker, T. Mihaljevic, R. G. Laurence, D. M. Dor, L. H. Cohn, M. G. Bawendi, J. V. Frangioni, *Nat. Biotechnol.* **2004**, *22*, 93.
[91] M. A. Hines, P. Guyot-Sionnest, *J. Phys. Chem. B* **1998**, *102*, 3655.
[92] a) Z. A. Peng, X. Peng, *J. Am. Chem. Soc.* **2001**, *123*, 183; b) L. Qu, Z. A. Peng, X. Peng, *Nano Lett.* **2001**, *1*, 333; c) W. W. Yu, X. Peng, *Angew. Chem.* **2002**, *114*, 2474; *Angew. Chem. Int. Ed.* **2002**, *41*, 2368.
[93] I. Mekis, D. V. Talapin, A. Kornowski, M. Haase, H. Weller, *J. Phys. Chem. B* **2003**, *107*, 7454.
[94] J. Jasieniak, C. Bullen, J. van Embden, P. Mulvaney, *J. Phys. Chem. B* **2005**, *109*, 20665.
[95] Y. A. Yang, H. Wu, K. R. Williams, Y. C. Cao, *Angew. Chem.* **2005**, *117*, 6870; *Angew. Chem. Int. Ed.* **2005**, *44*, 6712.
[96] a) J. M. Pietryga, R. D. Schaller, D. Werder, M. H. Stewart, V. I. Klimov, J. A. Hollingsworth, *J. Am. Chem. Soc.* **2004**, *126*, 11752; b) W. Lu, J. Fang, K. L. Stokes, J. Lin, *J. Am. Chem. Soc.* **2004**, *126*, 11798; c) B. L. Wehrenberg, C. Wang, P. Guyot-Sionnest, *J. Phys. Chem. B* **2002**, *106*, 10634; d) W. W. Yu, J. C. Falkner, B. S. Shih, V. L. Colvin, *Chem. Mater.* **2004**, *16*, 3318; e) L. S. Li, N. Pradhan, Y. Wang, X. Peng, *Nano Lett.* **2004**, *4*, 2261.
[97] N. Pradhan, S. Efrima, *J. Am. Chem. Soc.* **2003**, *125*, 2050.
[98] B. K. H. Yen, A. Günther, M. A. Schmidt, K. F. Jensen, M. G. Bawendi, *Angew. Chem.* **2005**, *117*, 5583; *Angew. Chem. Int. Ed.* **2005**, *44*, 5447.
[99] J. J. Li, Y. A. Wang, W. Guo, J. C. Keay, T. D. Mishima, M. B. Johnson, X. Peng, *J. Am. Chem. Soc.* **2003**, *125*, 12567.
[100] R. Xie, U. Kolb, J. Li, T. Basché, A. Mews, *J. Am. Chem. Soc.* **2005**, *127*, 7480.
[101] D. Pan, Q. Wang, S. Jiang, X. Ji, L. An, *Adv. Mater.* **2005**, *17*, 176.
[102] Y. C. Cao, J. Wang, *J. Am. Chem. Soc.* **2004**, *126*, 14336.
[103] J. H. Yu, J. Joo, H. M. Park, S. I. Baik, Y. W. Kim, S. C. Kim, T. Hyeon, *J. Am. Chem. Soc.* **2005**, *127*, 5662.
[104] R. Xie, X. Zhong, T. Basché, *Adv. Mater.* **2005**, *17*, 2741.
[105] J. S. Steckel, S. Coe-Sullivan, V. Bulović, M. G. Bawendi, *Adv. Mater.* **2003**, *15*, 1862.
[106] A. J. Houtepen, K. Rolf, D. Vanmaekelbergh, J. Meeldijk, S. G. Hickey, *J. Am. Chem. Soc.* **2006**, *128*, 6792.

[107] L. Cademartiri, G. von Freymann, A. C. Arsenault, J. Bertolotti, D. S. Wiersma, V. Kitaev, G. A. Ozin, *Small* **2005**, *1*, 1184.
[108] T. H. Larsen, M. Sigman, A. Ghezelbash, R. C. Doty, B. A. Korgel, *J. Am. Chem. Soc.* **2003**, *125*, 5638.
[109] M. B. Sigman, A. Ghezelbash, T. Hanrath, A. E. Saunders, F. Lee, B. A. Korgel, *J. Am. Chem. Soc.* **2003**, *125*, 16050.
[110] H. T. Zhang, G. Wu, X. H. Chen, *Langmuir* **2005**, *21*, 4281.
[111] Z. Liu, J. Liang, D. Xu, J. Lu, Y. Qian, *Chem. Commun.* **2004**, 2724.
[112] Y. Yin, R. M. Rioux, C. K. Erdonmez, S. Hughes, G. A. Somorjai, A. P. Alivisatos, *Science* **2004**, *304*, 711.
[113] J. R. Heath, J. J. Shiang, *Chem. Soc. Rev.* **1998**, *27*, 65.
[114] a) O. I. Mićić, C. J. Curtis, K. M. Jones, J. R. Sprague, A. J. Nozik, *J. Phys. Chem.* **1994**, *98*, 4966; b) O. I. Mićić, J. R. Sprague, C. J. Curtis, K. M. Jones, J. L. Machol, A. J. Nozik, H. Giessen, B. Fluegel, G. Mohs, N. Peyghambarian, *J. Phys. Chem.* **1995**, *99*, 7754.
[115] a) O. I. Mićić, J. Sprague, Z. Lu, A. J. Nozik, *Appl. Phys. Lett.* **1996**, *68*, 3150; b) D. V. Talapin, N. Gaponik, H. Borchert, A. L. Rogach, M. Haase, H. Weller, *J. Phys. Chem. B* **2002**, *106*, 12659.
[116] a) D. Battaglia, X. Peng, *Nano Lett.* **2002**, *2*, 1027; b) D. W. Lucey, D. J. MacRae, M. Furis, Y. Sahoo, A. N. Cartwright, P. N. Prasad, *Chem. Mater.* **2005**, *17*, 3754.
[117] S. Xu, S. Kumar, T. Nann, *J. Am. Chem. Soc.* **2006**, *128*, 1054.
[118] A. A. Guzelian, U. Banin, A. V. Kadavanich, X. Peng, A. P. Alivisatos, *Appl. Phys. Lett.* **1996**, *69*, 1432.
[119] Y. Cao, U. Banin, *J. Am. Chem. Soc.* **2000**, *122*, 9692.
[120] a) M. T. Reetz, E. Westermann, *Angew. Chem.* **2000**, *112*, 170; *Angew. Chem. Int. Ed.* **2000**, *39*, 165; b) M. Zhao, R. M. Crooks, *Angew. Chem.* **1999**, *111*, 375; *Angew. Chem. Int. Ed.* **1999**, *38*, 364; c) S.-A. Lee, K.-W. Park, B.-K. Kwon, Y.-E. Sung, *J. Ind. Eng. Chem.* **2003**, *9*, 63; d) K.-W. Park, Y.-E. Sung, *J. Ind. Eng. Chem.* **2006**, *12*, 165.
[121] a) M. C. Daniel, D. Astruc, *Chem. Rev.* **2004**, *104*, 293; b) R. Elghanian, J. J. Storhoff, R. C. Mucic, R. L. Letsinger, C. A. Mirkin, *Science* **1997**, *277*, 1078; c) Y. W. C. Cao, R. Jin, C. A. Mirkin, *Science* **2002**, *297*, 1536; d) S. J. Park, T. A. Taton, C. A. Mirkin, *Science* **2002**, *295*, 1503; e) C. M. Niemeyer, *Angew. Chem.* **2001**, *113*, 4254; *Angew. Chem. Int. Ed.* **2001**, *40*, 4128.
[122] a) G. Schmid, *Chem. Rev.* **1992**, *92*, 1709; b) H. Bönnemann, R. M. Richards, *Eur. J. Inorg. Chem.* **2001**, 2455; c) G. Schmid, *Clusters and Colloids*, VCH, New York, **1994**; d) G. Schmid, B. Corain, *Eur. J. Inorg. Chem.* **2003**, 3081; e) G. Schmid, M. Bäumle, M. Geerkens, I. Heim, C. Osemann, T. Sawitowski, *Chem. Soc. Rev.* **1999**, *28*, 179.
[123] a) M. Brust, A. Walker, D. Bethell, D. J. Schiffrin, R. Whyman, *J. Chem. Soc. Chem. Commun.* **1994**, 801; b) M. Brust, J. Fink, D. Bethell, D. J. Schiffrin, C. J. Kiely, *J. Chem. Soc. Chem. Commun.* **1995**, 1655; c) I. Hussain, S. Graham, Z. Wang, B. Tan, D. C. Sherrington, S. P. Rannard, A. I. Cooper, M. Brust, *J. Am. Chem. Soc.* **2005**, *127*, 16398; d) N. Zheng, J. Fan, G. D. Stucky, *J. Am. Chem. Soc.* **2006**, *128*, 6550.
[124] a) A. C. Templeton, W. P. Wuelfing, R. W. Murray, *Acc. Chem. Res.* **2000**, *33*, 27; b) S. Chen, K. Huang, J. A. Stearns, *Chem. Mater.* **2000**, *12*, 540.
[125] T. Shimizu, T. Teranishi, S. Hasegawa, M. Miyake, *J. Phys. Chem. B* **2003**, *107*, 2719.
[126] a) S. I. Stoeva, K. J. Klabunde, C. M. Sorensen, I. Dragieva, *J. Am. Chem. Soc.* **2002**, *124*, 2305; b) B. L. V. Prasad, S. L. Stoeva, C. M. Sorensen, K. J. Klabunde, *Chem. Mater.* **2003**, *15*, 935; c) B. L. V. Prasad, S. L. Stoeva, C. M. Sorensen, K. J. Klabunde, *Langmuir* **2002**, *18*, 7515.
[127] a) S. L. Stoeva, B. L. V. Prasad, S. Uma, S. P. K. Stoimenov, V. Zaikovsky, C. M. Sorensen, K. J. Klabunde, *J. Phys. Chem. B* **2003**, *107*, 7441; b) X. M. Lin, G. M. Wang, C. M. Sorensen, K. J. Klabunde, *J. Phys. Chem. B* **1999**, *103*, 5488; c) X. M. Lin, H. M. Jaeger, C. M. Sorensen, K. J. Klabunde, *J. Phys. Chem. B* **2001**, *105*, 3353.
[128] A. B. Smetana, K. J. Klabunde, C. M. Sorensen, A. A. Ponce, B. Mwale, *J. Phys. Chem. B* **2006**, *110*, 2155.
[129] a) N. Toshima, Y. T. Yonezawa, *New J. Chem.* **1998**, *22*, 1179; b) N. Toshima, K. Hirakawa, *Polymer J.* **1999**, *31*, 1127.
[130] Y. Sun, Y. Xia, *Science* **2002**, *298*, 2176.
[131] S. H. Im, Y. T. Lee, B. Wiley, Y. Xia, *Angew. Chem.* **2005**, *117*, 2192; *Angew. Chem. Int. Ed.* **2005**, *44*, 2154.
[132] a) J. Chen, B. Wiley, Z. Y. Li, D. Campbell, F. Saeki, H. Cang, L. Au, J. Lee, X. Li, Y. Xia, *Adv. Mater.* **2005**, *17*, 2255; b) Y. Sun, Y. Xia, *J. Am. Chem. Soc.* **2004**, *126*, 3892; c) H. Cang, T. Sun, J. Chen, B. Wiley, Z. Y. Li, Y. Xia, X. Li, *Opt. Lett.* **2005**, *30*, 3048.
[133] F. Kim, S. Connor, H. Song, T. Kuykendall, P. Yang, *Angew. Chem.* **2004**, *116*, 3759; *Angew. Chem. Int. Ed.* **2004**, *43*, 3673.
[134] A. Tao, P. Sinsermsuksakul, P. Yang, *Angew. Chem.* **2006**, *118*, 4713; *Angew. Chem. Int. Ed.* **2006**, *45*, 4597.
[135] X. Z. Lin, X. Teng, H. Yang, *Langmuir* **2003**, *19*, 10081.
[136] T. Teranishi, M. Miyake, *Chem. Mater.* **1998**, *10*, 594.
[137] P. Lu, T. Teranishi, K. Asakura, M. Miyake, N. Toshima, *J. Phys. Chem. B* **1999**, *103*, 9673.
[138] T. Herricks, J. Chen, Y. Xia, *Nano Lett.* **2004**, *4*, 2367.
[139] J. Chen, T. Herricks, Y. Xia, *Angew. Chem.* **2005**, *117*, 2645; *Angew. Chem. Int. Ed.* **2005**, *44*, 2589.
[140] Y. Xiong, J. Chen B. Wiley Y. Xia, S. Aloni, Y. Yin, *J. Am. Chem. Soc.* **2005**, *127*, 7332.
[141] a) Y. Xiong, J. Chen, B. Wiley, Y. Xia, Y. Yin, Z. Y. Li, *Nano Lett.* **2005**, *5*, 1237; b) Y. Xiong, B. Wiley, J. Chen, Z. Y. Li, Y. Yin, Y. Xia, *Angew. Chem.* **2005**, *117*, 8127; *Angew. Chem. Int. Ed.* **2005**, *44*, 7913; c) Y. Xiong, J. M. McLellan, J. Chen, Y. Yin, Z. Y. Li, Y. Xia, *J. Am. Chem. Soc.* **2005**, *127*, 17118.
[142] H. Song, F. Kim, S. Connor, G. A. Somorjai, P. Yang, *J. Phys. Chem. B* **2005**, *109*, 188.
[143] J. D. Hoefelmeyer, K. Niesz, G. A. Somorjai, T. D. Tilley, *Nano Lett.* **2005**, *5*, 435.
[144] S. W. Kim, J. Park, Y. Jang, Y. Chung, S. Hwang, T. Hyeon, Y. W. Kim, *Nano Lett.* **2003**, *3*, 1289.
[145] S. U. Son, Y. Jang, K. Y. Yoon, E. Kang, T. Hyeon, *Nano Lett.* **2004**, *4*, 1147.
[146] S. U. Son, Y. Jang, J. Park, H. B. Na, H. M. Park, H. J. Yun, J. Lee, T. Hyeon, *J. Am. Chem. Soc.* **2004**, *126*, 5026.
[147] a) K. Pelzer, O. Vidoni, K. Philippot, B. Chaudret, V. Collière, *Adv. Funct. Mater.* **2003**, *13*, 118; b) C. Pen, K. Pelzer, K. Philippot, B. Chaudret, F. Dassenoy, P. Lecanate, M. J. Casanove, *J. Am. Chem. Soc.* **2001**, *123*, 7584.
[148] a) G. Viau, R. Brayner, L. Poul, N. Chakroune, E. Lacaze, F. Fiévet-Vincent, F. Fiévet, *Chem. Mater.* **2003**, *15*, 486; b) N. Chakroune, G. Viau, S. Ammar, L. Poul, D. Veautier, M. M. Chehimi, C. Mangeney, F. Villain, F. Fiévet, *Langmuir* **2005**, *21*, 6788.
[149] C. Pan, F. Dassenoy, M. J. Casanove, K. Philippot, C. Amiens, P. Lecante, A. Mosset, B. Chaudret, *J. Phys. Chem. B* **1999**, *103*, 10098.
[150] C. A. Stowell, B. A. Korgel, *Nano Lett.* **2005**, *5*, 1203.
[151] a) E. V. Shevchenko, D. V. Talapin, C. B. Murray, S. O'Brien, *J. Am. Chem. Soc.* **2006**, *128*, 3620; b) J. J. Urban, D. V. Talapin, E. V. Shevchenko, C. B. Murray, *J. Am. Chem. Soc.* **2006**, *128*, 3248; c) E. V. Shevchenko, D. V. Talapin, N. A. Kotov, S. O'Brien, C. B. Murray, *Nature* **2006**, *439*, 55; d) E. V. Shevchenko, D. V. Talapin, S. O'Brien, C. B. Murray, *J. Am. Chem. Soc.* **2005**, *127*, 8741; e) F. X. Redl, K.-S. Cho, C. B. Murray, S. O'Brien, *Nature* **2003**, *423*, 968; f) A. Courty, A. Mermet, P. A. Albouy, E. Duval, M. P. Pileni, *Nat. Mater.* **2005**, *4*, 395; g) A. Courty, C. Fermon, M. P. Pileni, *Adv. Mater.* **2001**, *13*, 254; h) J. Legrand, A. T. Ngo, C. Petit, M. P. Pileni, *Adv. Mater.* **2001**, *13*, 58; i) A. M. Kalsin, M. Fialkowski, M. Paszewski, S. K. Smoukov, K. J. M. Bishop, B. A. Grzybowski, *Science* **2006**, *312*, 420;

j) H. Y. Fan, K. Yang, D. Boye, T. Sigmon, K. Malloy, H. Xu, G. P. Lopez, C. Brinker, *Science* **2004**, *304*, 567; k) H. Y. Fan, E. Leve, J. Gabaldon, A. Wright, R. E. Haddad, C. J. Brinker, *Adv. Mater.* **2005**, *17*, 2587.

[152] a) C. M. Niemeyer, C. A. Mirkin, *Nanobiotechnology: Concepts, Applications and Perspectives*, Wiley-VCH, Weinheim, **2004**; b) J. Wang, *Small* **2005**, *1*, 1036.

[153] a) R. Weissleder, K. Kelly, E. Y. Sun, T. Shtatland, L. Josephson, *Nat. Biotechnol.* **2005**, *23*, 1418; b) J. W. M. Bulte, S. C. Zhang, P. van Gelderen, V. Herynek, E. K. Jordan, I. D. Duncan, J. A. Frank, *Proc. Natl. Acad. Sci. USA* **1999**, *96*, 15256; c) Y. W. Jun, Y. M. Huh, J. S. Choi, J. H. Lee, H. T. Song, S. Kim, S. Yoon, K. S. Kim, J. S. Shin, J. S. Suh, J. Cheon, *J. Am. Chem. Soc.* **2005**, *127*, 5732; d) H. Gu, P. L. Ho, K. W. T. Tsang, L. Wang, B. Xu, *J. Am. Chem. Soc.* **2003**, *125*, 15702; e) C. Xu, K. Xu, H. Gu, X. Zhong, Z. Guo, R. Zheng, X. Zhang, B. Xu, *J. Am. Chem. Soc.* **2004**, *126*, 3392; f) J. Won, M. Kim, Y. W. Yi, Y. H. Kim, N. Jung, T. K. Kim, *Science* **2005**, *309*, 121; g) C. Xu, K. Xu, H. Gu, R. Zheng, H. Liu, X. Zhang, Z. Guo, B. Xu, *J. Am. Chem. Soc.* **2004**, *126*, 9938.

[154] a) B. Dubertret, P. Skourides, D. J. Norris, V. Noireaux, A. H. Brivanlou, A. Libchaber, *Science* **2002**, *298*, 1759; b) I. L. Medintz, H. T. Uyeda, E. R. Goldman, H. Mattoussi, *Nat. Mater.* **2005**, *4*, 435; c) X. Michalet, F. F. Pinaud, L. A. Bentolila, J. M. Tsay, S. Doose, J. J. Li, G. Sundaresan, A. M. Wu, S. S. Gambhir, S. Weiss, *Science* **2005**, *307*, 538; d) J. M. Klostranec, W. C. W. Chan, *Adv. Mater.* **2006**, *18*, 1953.

[155] a) T. A. Taton, C. A. Mirkin, R. L. Letsinger, *Science* **2000**, *289*, 1757; b) J. M. Nam, C. S. Thaxton, C. A. Mirkin, *Science* **2003**, *301*, 1884.

[156] a) T. Pellegrino, S. Kudera, T. Liedl, A. M. Javier, L. Manna, W. J. Parak, *Small* **2005**, *1*, 49; b) Challa S. S. R. Kumar, *Biofunctionalization of Nanomaterials*, Wiley-VCH, Weinheim, **2005**.

[157] a) J. Kim, J. E. Lee, J. Lee, Y. Jang, S. W. Kim, K. An, J. H. Yu, T. Hyeon, *Angew. Chem.* **2006**, *118*, 4907; *Angew. Chem. Int. Ed.* **2006**, *45*, 4789; b) J. Kim, J. E. Lee, J. Lee, J. H. Yu, B. C. Kim, K. An, Y. Hwang, C. H. Shin, J. G. Park, J. Kim, T. Hyeon, *J. Am. Chem. Soc.* **2006**, *128*, 688; c) J. Kim, S. Park, J. E. Lee, S. M. Jin, J. H. Lee, I. S. Lee, I. Yang, J.-S. Kim, S. K. Kim, M.-H. Cho, T. Hyeon, *Angew. Chem.* **2006**, *118*, 7918; *Angew. Chem. Int. Ed.* **2006**, *45*, 7754.

